

Inflation, String Theory and Cosmic Strings

David F. Chernoff

Department of Astronomy, Cornell University, Ithaca, New York

S.-H. Henry Tye

*Jockey Club Institute for Advanced Study and Department of Physics, Hong Kong University of Science and Technology, Clear Water Bay, Hong Kong and
Department of Physics, Cornell University, Ithaca, New York*

ABSTRACT: At its very beginning, the universe is believed to have grown exponentially in size via the mechanism of inflation. The almost scale-invariant density perturbation spectrum predicted by inflation is strongly supported by cosmological observations, in particular the cosmic microwave background radiation. However, the universe's precise inflationary scenario remains a profound problem for cosmology and for fundamental physics. String theory, the most-studied theory as the final physical theory of nature, should provide an answer to this question. Some of the proposals on how inflation is realized in string theory are reviewed. Since everything is made of strings, some string loops of cosmological sizes are likely to survive in the hot big bang that followed inflation. They appear as cosmic strings, which can have intricate properties. Because of the warped geometry in flux compactification of the extra spatial dimensions in string theory, some of the cosmic strings may have tensions substantially below the Planck or string scale. Such strings cluster in a manner similar to dark matter leading to hugely enhanced densities. As a result, numerous fossil remnants of the low tension cosmic strings may exist within the galaxy. They can be revealed through the optical lensing of background stars in the near future and studied in detail through gravitational wave emission. We anticipate that these cosmic strings will permit us to address central questions about the properties of string theory as well as the birth of our universe.

For: Quantum Gravity Part of One Hundred Years of General Relativity: From Genesis and Empirical Foundations to Gravitational Waves, Cosmology and Quantum Gravity

Contents

1. Introduction	2
2. The Inflationary Universe	5
3. String Theory and Inflation	8
3.1 String Theory and Flux Compactification	8
3.2 Inflation in String Theory	10
4. Small r Scenarios	12
4.1 Brane Inflation	12
4.2 Kähler Moduli Inflation	16
5. Large r Scenarios	17
5.1 The Kim-Nilles-Peloso Mechanism	17
5.2 Axion Monodromy	20
5.3 Discussions	21
6. Relics: Low Tension Cosmic Strings	23
6.1 Strings in Brane World Cosmology	24
6.2 Current Bounds on String Tension $G\mu$ and Probability of Intercommutation p	25
7. Scaling, Slowing, Clustering and Evaporating	28
7.1 Large-scale String Distribution	31
7.2 Local string distribution	34
8. Detection	38
8.1 Detection via Microlensing	38
8.2 WFIRST Microlensing Rates	40
8.3 Gravitational Waves	42

1. Introduction

By 1930, quantum mechanics, general relativity and the Hubble expansion of our universe were generally accepted by the scientific community as 3 triumphs of modern physical science. Particles and fields obey quantum mechanical rules and space-time bends and warps according to Einstein's classical description of gravity. The dynamical arena for particles, fields and space-time is the universe and modern cosmology is born as the application of these physical laws to the universe itself.

The path forward seemed clear but in the 1950s and 1960s physicists first began to appreciate that trying to quantize the classical gravitational field led to severe inconsistencies. This non-renormalizability problem was further sharpened once the quantization of gauge (vector) fields was well understood in early 1970s.

At about the same time, string theory – a quantum mechanical theory of one-dimensional objects – was found to contain a graviton (a massless spin-2 particle). The promise of a self-consistent theory of quantum gravity has attracted huge attention since the 1980s. Tremendous progress has been made in the past 30 years in understanding many aspects of string theory; yet today we are no closer to knowing which of many theoretical possibilities might describe our universe and we still lack experimental evidence that the theory describes nature.

By now, string theory is such a large topic with so many research directions that we have to choose a specific area to discuss. The centenary of general relativity prompts us to reflect on 2 very amazing manifestations of general relativity: namely black holes and cosmology. Given the tremendous progress in cosmology in the past decades, both in observation and in theory, we shall focus here on the intersection of string theory and cosmology.

Our fundamental understanding of microscopic physics is grounded in quantum field theory and gravity but if we hope to work at very high energies then we cannot escape the need for an ultraviolet completion to these theories. String theory provides a suitable framework. The string scale M_S is expected to be below the reduced Planck scale $M_{Pl} = 1/\sqrt{8\pi G} \simeq 2.4 \times 10^{18}$ GeV (where G is the Newton's constant) but not too far from the grand unified scale $M_{GUT} \simeq 10^{16}$ GeV (where the proton mass is about 1 GeV, in units where $c = \hbar = 1$). Particle physics properties at scales much lower than M_S are hard to calculate within our present understanding of string theory. High energy experiments can reach only multi-TeV scales, orders of magnitude below the expected M_S . The difficulty of finding a common arena to compare theory and observation is hardly a new dilemma: although standard quantum mechanics works well at and above eV energy scales, it is woefully inadequate to describe properties of proteins which typically involve milli-eV scales and lower. Where should we look?

One place to look for stringy effects is in the early universe. If the energy scale of the early universe reaches M_S , an abundance of physical effects will provide a

more direct path to test our ideas than currently feasible in high energy experiments. In fact, attempts to interpret observations will tell us whether our present understanding of physics and the universe is advanced enough to permit us to ask and answer sensible questions about these remote physical regimes. We shall focus on the inflationary universe scenario [1, 2, 3], which reaches energy scales sufficiently high to create ample remnants. The hot big bang’s nucleosynthetic epoch has direct observational support at and below MeV scales whereas the energies of interest to us are $\sim M_S$. We are most fortunate that precision cosmology has begun to let us address questions relevant to these extreme conditions. Even in this rather specialized topic of inflationary cosmology and string theory, a comprehensive review by Baumann and McAllister [4] appeared recently. So we shall take the opportunity here to present a brief introduction and share within this framework some of our own views on a particularly interesting topic, namely, cosmic strings. The subject of cosmic strings has been extensively studied too [5], so here we shall focus on low tension cosmic strings, which may appear naturally in string theory.

There are many specific ways to realize inflation within string theory. These may be roughly grouped into models with small and large field ranges. They have rather different properties and predictions. Recall that 6 of the 9 spatial dimensions must be compactified into a Calabi-Yau like manifold with volume V_6 , where

$$\left(\frac{M_{Pl}}{M_S}\right)^2 \sim M_S^6 V_6 \gg 1. \quad (1.1)$$

During inflation the inflaton field ϕ moves from an initial to final position within the manifold, covering a path or field range $\Delta\phi$. Now, the distance scale inside the compactified manifold is bounded by M_{Pl} . The case $\Delta\phi < M_{Pl}$ is known as small field inflation. The opposite limit when the field range far exceeds the typical scale of the manifold, $\Delta\phi \gg M_{Pl}$, is large field inflation. In the latter case the inflaton wanders inside the compactified manifold for a while during inflation. This scenario may occur if the inflaton is an axion-like field and executes a helical-like motion. Flux compactification of the 6 spatial dimensions in string theory typically introduces many axions and naturally sets the stage for this possibility.

The recent B-mode polarization measurement in the cosmic microwave background (CMB) radiation [6] by BICEP2 is most interesting. Primordial B-mode polarization is sourced by tensor perturbations during inflation and measurable primordial B-mode polarization implies that $\Delta\phi \gg M_{Pl}$. This is a prototypical example of how it’s now possible to probe high energies and early moments of the universe’s history by means of cosmological observations. However, since dust can contaminate today’s observed signal [7, 8], it remains to be seen whether the BICEP2 observations definitively imply that large field inflation takes place. We believe this issue should be settled soon. In the meantime, we shall entertain both possibilities here.

In both small and large field ranges macroscopic, one-dimensional objects, hereafter cosmic strings, can appear rather naturally. In the former case, the cosmic strings can be the fundamental superstrings themselves, while in the latter case, they can be fundamental strings and/or vortices resulting from the Higgs like mechanism. Cosmic strings with tension above the inflation scale will not be produced after inflation and we should expect only relatively low tension strings to be produced. Because of the warped geometry and the presence of throats in the compactification in string theory, some cosmic strings can acquire very low tensions. In flux compactification such strings tend to have nontrivial tension spectrum (and maybe even with beads).

If the cosmic string tension is close to the present observational bound (about $G\mu < 10^{-7}$), strings might contribute to the B-mode polarization at large ℓ multipoles independent of whether or not BICEP2 has detected primordial B mode signals. The string contribution to the CMB power spectrum of temperature fluctuations is limited to be no more than $\sim 10\%$ and this constrains any string B-mode contribution. Because the primordial tensor perturbation from inflation decreases quickly for large ℓ multipoles one very informative possibility is that cosmic strings are detected at large ℓ and other astrophysical contributions are sub-dominant.

On the other hand, if tension is low ($G\mu \ll 10^{-7}$) then the cosmic string effect for all ℓ is negligible compared to known sources and foreground contributions. Other signatures must be sought. For small $G\mu$ string loops are long lived and the oldest (and smallest) tend to cluster in our galaxy, resulting in an enhancement of $\sim 10^5$ in the local string density. This enhancement opens up particularly promising avenues for detecting strings by microlensing of stars within the galaxy and by gravitational wave emission in the tension range $10^{-14} < G\mu \ll 10^{-7}$. As a cosmic string passes in front of a star, its brightness typically doubles, as the 2 images cannot be resolved. As a string loop oscillates in front of a star, it generates a unique signature of repeated achromatic brightness doubling. Here we briefly review the various observational bounds on cosmic strings and estimate the low tension cosmic string density within our galaxy as well as the likelihood of their detection in the upcoming observational searches. It is encouraging that searches of extrasolar planets and variables stars also offer a chance to detect the micro-lensing of stars by cosmic strings. Once a location is identified by such a detection, a search for gravitational wave signals should follow.

Detection of cosmic strings followed by the measurement of their possible different tensions will go a long way in probing superstring theory. Although a single string tension can easily originate from standard field theory, a string tension spectrum should be considered as a distinct signature of string theory. It is even possible that some cosmic strings will move in the compactified dimensions with warped geometry, which can show up observationally as strings with varying tension, both along their lengths as well as in time. In summary, cosmic strings probably offer the best chance of finding distinct observational support for the string theory.

2. The Inflationary Universe

So far, observational data agrees well with the simplest version of the slow-roll inflationary universe scenario, i.e., a single, almost homogeneous and isotropic, scalar inflaton field $\phi = \phi(t)$ subject to potential $V(\phi)$. For a Friedmann-Lemaître-Robertson-Walker metric, general relativity yields simple equations for the cosmic scale factor $a(t)$ and for ϕ ,

$$H^2 = \left(\frac{\dot{a}}{a}\right)^2 = \frac{1}{3M_{Pl}^2} \left[V(\phi) + \frac{\dot{\phi}^2}{2} \right] + \frac{\rho_c(0)}{a^2} + \frac{\rho_m(0)}{a^3} + \frac{\rho_r(0)}{a^4} + \dots \quad (2.1)$$

$$\ddot{\phi} + 3H\dot{\phi} = -\frac{dV}{d\phi} = -V'(\phi) \quad (2.2)$$

where the Hubble parameter $H = \dot{a}/a$ ($\dot{a}(t) = da/dt$) measures the rate of expansion of the universe, and $\rho_c(0)$, $\rho_m(0)$ and $\rho_r(0)$ are the curvature, the matter and the radiation densities at time $t = 0$. In an expanding universe, $a(t)$ grows and the curvature, the matter and the radiation terms diminish. The energy and pressure densities for the inflaton are

$$\rho_\phi = \frac{\dot{\phi}^2}{2} + V(\phi) \quad (2.3)$$

$$p_\phi = \frac{\dot{\phi}^2}{2} - V(\phi)$$

where a canonical kinetic term for ϕ is assumed. If $V(\phi)$ is sufficiently flat and if $\dot{\phi}$ is initially small then Eq.(2.2) implies that ϕ moves slowly in the sense that its kinetic energy remains small compared to the potential energy, $\dot{\phi}^2 \ll V(\phi)$. In the limit that $V(\phi)$ is exactly constant and dominates in Eq.(2.1) then H is constant and $a(t) \propto e^{Ht}$. More precisely one may define the inflationary epoch as that period when the expansion of the universe is accelerating, i.e., $\ddot{a} > 0$, or, in a spatially flat universe,

$$2M_{Pl}^2 \dot{H} = -(\rho + p) \quad (2.4)$$

$$\epsilon = -\frac{\dot{H}}{H^2} = \frac{3}{2} \left(1 + \frac{p}{\rho} \right) < 1.$$

Slow-roll inflation means small ϵ , H nearly constant and $a(t) \sim a(0)e^{Ht}$.

In a typical slow-roll inflationary model inflation ends at $t = t_{end}$ when the inflaton encounters a steeper part of the potential and $\epsilon > 1$. The number of e-folds of inflation is $N_e \simeq Ht_{end}$, a key parameter. The energy released from the potential $V(\phi)$ heats the universe at the end of inflation and starts the hot big bang. The period of slow-roll must last at least $N_e > 50$ e-folds to explain three important observations about our universe that are otherwise unaccounted for in the normal

big bang cosmology: flatness, lack of defects and homogeneity. For any reasonable initial curvature density $\rho_c(0)$, the final curvature density $\rho_c(t_{end}) < \rho_c(0)e^{-150}$ will be totally negligible, thus yielding a flat universe. This is how inflation solves the flatness problem. Any defect density (probably included in $\rho_m(0)$) present in the universe before the inflationary epoch will also be inflated away, thus solving the so-called “monopole” or defect problem. Since the cosmic scale factor grows by a huge factor, the universe we inhabit today came from a tiny patch of the universe before inflation. Any original inhomogeneity will be inflated away. Inflation explains the high degree of homogeneity of the universe. In summary, if N_e is sufficiently large then inflation accounts for the universe’s observed flatness, defect density and homogeneity.

What is amazing is that inflation also automatically provides a mechanism to create primordial inhomogeneities that ultimately lead to structure formation in our universe. As the inflaton slowly rolls down the potential in the classical sense, quantum fluctuations yield slightly different ending times t_{end} and so slightly different densities in different regions. The scalar and the metric fluctuations may be treated perturbatively, and one obtains the dimensionless power spectra in terms of H ,

$$\begin{aligned}\Delta_S^2(k) &= \frac{1}{8\pi^2} \frac{H^2}{M_{Pl}^2 |\epsilon|} & (2.5) \\ \Delta_T^2(k) &= \frac{2}{\pi^2} \frac{H^2}{M_{Pl}^2} = r \Delta_S^2(k) \\ r &= 16\epsilon\end{aligned}$$

where Δ_S^2 and Δ_T^2 are the scalar and the tensor modes respectively. A scalar scale-invariant power spectrum corresponds to constant Δ_S^2 , which is the case for a pure de-Sitter space. The scalar mode is related to the temperature fluctuations first measured by COBE [9]. Measurements and modeling have been refined over the past 2 decades. Since ϕ rolls in the non-flat potential in the inflationary scenario, Δ_S^2 will have a slight k dependence. This is usually parametrized with respect to the pivot wave number k_p in the form

$$\Delta_S^2(k) = \Delta_S^2(k_p) (k/k_p)^{n_s-1+(dn_s/d\ln k)\ln(k/k_p)/2+\dots} \quad (2.6)$$

$$\Delta_T^2(k) = \Delta_T^2(k_p) (k/k_p)^{n_t+(dn_t/d\ln k)\ln(k/k_p)/2+\dots} \quad (2.7)$$

where the PLANCK and WMAP best fit values for Λ CDM quoted in Ref.[10] for $k_p = 0.05\text{Mpc}^{-1}$ are

$$n_s = 0.9603 \pm 0.0073 \quad (2.8)$$

$$\Delta_S^2(k_p) = 2.19_{-0.53}^{+0.58} \times 10^{-9}. \quad (2.9)$$

These do not change appreciably when a possible tensor component is included and PLANCK constraints on r are given at pivot 0.002 Mpc^{-1} . In the slow-roll approximation, where $\ddot{\phi}$ is negligible in Eq.(2.2), the deviation from scale-invariance is

quantified by the spectral tilt

$$n_s - 1 = \frac{d \ln \Delta_S^2(k)}{d \ln k} = -6\epsilon + 2\eta \quad (2.10)$$

$$\frac{dn_s}{d \ln k} = -16\epsilon\eta + 24\epsilon^2 + 2\xi^2$$

where the parameters that measure the deviation from flatness of the potential are

$$\epsilon = \frac{M_{Pl}^2}{2}(V'/V)^2, \quad (2.11)$$

$$\eta = M_{Pl}^2 V''/V, \quad (2.12)$$

$$\xi^2 = M_{Pl}^4 V'V'''/V^2.$$

where ϵ and η are the known as the slow-roll parameters which take small values during the inflationary epoch. The tensor mode comes from the quantum fluctuation of the gravitational wave. Its corresponding tilt is

$$n_t = -2\epsilon. \quad (2.13)$$

For a small field range $\Delta\phi$, the constraint on N_e dictates a rather flat potential and small ϵ , which in turn implies a very small r . This relation can be quantified by the Lyth bound, [11],

$$\frac{\Delta\phi}{M_{Pl}} \geq N_e \sqrt{r/8}. \quad (2.14)$$

If $60 \geq N_e \geq 40$, we find that typical values of r satisfies $r < 0.005$ for $\Delta\phi < M_{Pl}$. This is much smaller than $r \simeq 0.2$ reported by BICEP2 [6].

While Δ_S^2 is a combination of H^2 and $1/\epsilon$, Δ_T^2 provides a direct measurement of H^2 and hence the magnitude of the inflaton potential during inflation:

$$V \simeq \left(\frac{r}{0.2}\right) (2.2 \times 10^{16} \text{GeV})^4. \quad (2.15)$$

The imprint of tensor fluctuations are present in the CMB but $\Delta_T^2 \ll \Delta_S^2$ so it's not possible to measure Δ_T^2 directly from total temperature fluctuations. Fortunately, the CMB is linearly polarized and can be separated into E-mode and B-mode polarizations. It happens that Δ_T^2 contributes to both modes while Δ_S^2 contributes only to the E-mode. So a measurement of the primordial B-mode polarized CMB radiation is a direct measurement of Δ_T^2 .

Searching for the B-mode CMB is very important. Besides the intrinsic smallness of the B-mode signal, which makes detection a major challenge, the primordial fluctuation may be masked by the interstellar dust. It is likely that the uncertainty from dust would have been resolved by the time this article appears. So we may consider this as a snapshot after the announcement of the BICEP2 data and before a full understanding of the impact of dust on the reported detection. Due to this uncertainty, we shall consider both a negligibly small r (say $r < 0.002$) and an observable primordial $r \leq 0.2$.

3. String Theory and Inflation

By now, string theory is a huge research subject. So far, we have not yet identified the corner where a specific string theory solution fits what happens in nature. It is controversial to state whether we are close to finding that solution or we are still way off. By emphasizing the cosmological epoch, we hope to avoid the details but try to find generic stringy features that may show up in cosmological observations. Here we give a lightning pictorial summary of some of the key features of Type IIB superstring theory so readers can have at least a sketchy picture of how string theory may be tested.

Because of compactification, we expect modes such as Kaluza-Klein modes to appear in the effective 4-dimensional theory. Their presence will alter the relation between the inflaton potential scale and r (2.15) to :

$$V \simeq \frac{1}{\hat{N}^2} \left(\frac{r}{0.2} \right) (2.2 \times 10^{16} \text{GeV})^4. \quad (3.1)$$

where \hat{N} effectively counts the number of universally coupled (at one-loop) degrees of freedom below the energy scale of interest here [12]. Present experimental bound on \hat{N} is very loose. Surprisingly, a value as big as $\hat{N} \sim 10^{25}$ is not ruled out.

3.1 String Theory and Flux Compactification

Recall that 2-form electric and magnetic field strengths follow from the 1-form field A_μ in the electromagnetic theory, under which point-like particles (such as electrons) are charged. In analogy to this, fundamental strings in string theory are charged under a 2-form field $B_{\mu\nu}$ which yields 3-form field strengths. In general, other dimensional objects are also present in string theory, which are known as branes. A p-brane spans p spatial dimensions, so a membrane is a 2-brane while a 1-brane is string like; that is a 1-brane is really a string. In the Type IIB superstring theory, there are a special type of Dp -branes where p is an odd integer. Among other properties of Dp -branes, we like to mention two particularly relevant ones here : (1) each end of an open string must end on a Dp -brane, and (2) with the presence of $D1$ -string (or -brane), there exists another 2-form field $C_{\mu\nu}$ under which a $D1$ -string is charged.

Self-consistency of Type IIB superstring theory requires it to have 9 spatial dimensions. Since only 3 of them describe our observable world, the other 6 must be compactified. Consider a stack of $D3$ -branes of cosmological size. Such a stack appear as a point in the 6 compactified dimensions. In the brane world scenario, all standard model particles (electrons, quarks, gluons, photons, et. al.) are light open string modes whose ends can move freely inside the $D3$ -branes, but cannot move outside the branes, while the graviton, being a closed string mode, can move freely in the branes as well as outside, i.e., the bulk region of the 6 compactified dimensions.

In this sense, the $D3$ -branes span our observable universe. We can easily replace the $D3$ -branes by $D7$ -branes, with 4 of their dimensions wrapping a 4-cycle inside the compactified 6-dimensional space. Dark matter may come from unknown particles inside the same stack, or from open string modes sitting in another stack sitting somewhere else in the compactified space.

As a self-consistent theory, the 6 extra dimensions must be dynamically compactified (and stabilized). This is a highly non-trivial problem. Fortunately, the 3-form field strengths of both the NS-NS field $B_{\mu\nu}$ and the R-R field $C_{\mu\nu}$ are quantized in string theory. Wrapping 3-cycles in the compactified dimensions, these fluxes contribute to the effective potential V in the low energy approximation. Their presence can render the shape and the size of the compactified 6-dimensional space to be dynamically stabilized. This is known as flux compactification. Here the matter content and the forces of nature are dictated by the specific flux compactification [13, 14]. Warped internal space appears naturally. This warped geometry will come to play an important role in cosmology.

To describe nature, a Calabi-Yau like manifold is expected, with branes and orientifold planes. At low energy, a particular manifold may be described by a set of dynamically stabilized scalar fields, or moduli. One or more Kähler moduli parameterize the volume while the shape is described by the complex structure moduli, whose number may reach hundreds. A typical flux compactification involves many moduli and three-form field strengths with quantized fluxes (see the review [15]). With such a large set of dynamical ingredients, we expect many possible vacuum solutions; collectively, this is the string theory landscape, or the so-called cosmic landscape. Here, a modulus is a complex scalar field. Written in polar coordinate, we shall refer to the phase degree of freedom as an axion.

For a given Calabi-Yau like manifold, we can, at least in principle, determine the four-dimensional low energy supergravity effective potential V for the vacua. To be specific, let us consider only 3-form field strengths F_3^i wrapping the three-cycles inside the manifold. (Note that these are dual to the four-form field strengths in 4 dimensional space-time.) We have $V(F_3^i, \phi_j) \rightarrow V(n_i, \phi_j)$, ($i = 1, 2, \dots, N$, $j = 1, 2, \dots, K$) where the flux quantization property of the 3-form field strengths F_3^i allow us to rewrite V as a function of the quantized values n_i of the fluxes present and ϕ_j are the complex moduli describing the size and shape of the compactified manifold as well as the couplings. There are barriers between different sets of flux values. For example, there is a (finite height) barrier between n_1 and $n_1 - 1$, where tunneling between $V(n_1, n_2, \dots, n_N, \phi_j)$ and $V(n_1 - 1, n_2, \dots, n_N, \phi_j)$ may be achieved by brane-flux annihilation [16]. For a given set of n_i , we can locate the meta-stable (classically stable) vacuum solutions $V(n_i, \phi_j)$ by varying ϕ_j . We sift through these local minima which satisfy the following criteria: they have vanishingly small vacuum energies because that is what is observed in today's universe, and long decay lifetimes to lower energy states because our universe is long-lived. These criteria restrict the

manifolds, flux values and minima of interest; nonetheless, within the rather crude approximation we are studying, there still remain many solutions; and statistically, it seems that a very small cosmological constant is preferred [17].

3.2 Inflation in String Theory

When the universe was first created (say, a bubble created via tunneling from nothing), ϕ_j are typically not sitting at $\phi_{j,\min}$, so they tend to roll towards their stabilized values. Heavier moduli with steeper gradients probably reached their respective minima relatively quickly. The ones with less steep directions took longer. The last ones to reach their stabilized values typically would move along relatively flat directions, and they can play the role of inflatons. So the vacuum energy that drives inflation is roughly given by the potential when all moduli except the inflaton have already reached bottom. Since the flux compactification in string theory introduces dozens or hundreds of moduli (each is a complex scalar field in the low energy effective theory approximation), one anticipates that there are many candidates for inflation. Even if we assume that just one field is responsible for the inflationary epoch in our own universe it seems likely that string theory can choose among many possibilities to realize single field inflation in many different ways.

In fact, the picture from string theory may offer additional interesting possibilities beyond field theory. For example, suppose there was a pair of brane-anti-brane present in the early universe whose tensions drive the inflation. As we shall see, the inflaton field happens to be the distance between them. After their annihilation that ends inflation, the inflaton field no longer exists as a degree of freedom in the low energy effective field theory.

Some inflationary scenarios in string theory generate unobservably small primordial r while others give observably large primordial r . Small field range implies small r , but large field range does not necessarily imply large r , which happens when the Lyth bound (2.14) is not saturated. To obtain enough e-folds, we need a flat enough potential, so it is natural to consider an axion as the inflaton, as first proposed in natural inflation [18, 19]. The axion has a natural shift symmetry $\phi \rightarrow \phi + \text{any constant}$. This continuous symmetry can easily be broken, via non-perturbative effects, to a discrete symmetry, resulting in a periodic potential that can drive inflation. The typical field range is sub-Planckian implying a small r . We shall see shortly that there are many string theory models built out of the axion that permit large field ranges and some of these can yield large r .

Here, we shall describe the various string theory realization of inflation within the framework of Type IIB string theory. The pictorially simplest models occur in the brane world scenario. We shall present a few sample models to give a picture of the type of models that have been put forward. Readers can find a more complete list in Ref.[4]. If r turns out to be large, it will be interesting to see whether some of the small r models can be adapted or modified to have a large r . For example,

one can try to modify a brane inflationary scenario into a warm inflationary scenario with a relatively large r .

4. Small r Scenarios

Besides fundamental superstrings, Type IIB string theory has Dp -branes where the number of spatial dimensions p is odd. Furthermore, supersymmetry can be maintained if there are only $D3$ - and $D7$ -branes; so, unless specified otherwise, we shall restrict ourselves to this case. String theory has 9 spatial dimensions. Since our observable universe has only 3 spatial dimensions, the other 6 spatial dimensions have to be compactified in a manifold with volume V_6 . The resulting (i.e., dynamically derived) M_{Pl} is related to the string scale M_S via Eq.(1.1) and the typical field range $\Delta\phi$ is likely to be limited by $M_{Pl} > M_S$. For such a small field range, the potential has to be flat enough to allow 50 or more e-folds and the Lyth bound (2.14) for $60 \geq N_e \geq 40$ implies $r < 0.005$. We shall refer to these models as small r scenarios.

4.1 Brane Inflation

The discovery of branes in string theory actually renders the string theory to a theory of extended objects. In the brane world scenario, our visible universe lies inside a stack of $D3$ -branes, or a stack of $D7$ -branes. Here, 6 of the 9 spatial dimensions are dynamically compactified while the 3 spatial dimensions of the $D3$ -branes (or 3 of the $D7$ -branes) are cosmologically large. The 6 small dimensions are stabilized via flux compactification [13, 14]; the region outside the branes is referred to as the bulk region. The presence of RR and NS-NS fluxes introduces intrinsic torsion and warped geometry, so there are regions in the bulk with warped throats (Figure 1). Since each end of an open string must end on a brane, only closed strings are present in the bulk away from branes.

There are numerous such solutions in string theory, some with a small positive vacuum energy (cosmological constant). Presumably the standard model particles are open string modes; they can live either on $D7$ -branes wrapping a 4-cycle in the bulk or (anti-) $D3$ -branes at the bottom of a warped throat (Figure 1). The (relative) position of a brane is an open string mode. In brane inflation [20], one of these modes is identified as the inflaton ϕ , while the inflaton potential is generated by the classical exchange of closed string modes including the graviton. From the open string perspective, this exchange of a closed string mode can be viewed as a quantum loop effect of the open string modes.

$D3$ - $\bar{D}3$ -brane Inflation

In the early universe, besides all the branes that are present today, there is an extra pair of $D3$ - $\bar{D}3$ -branes [21, 22]. Due to the attractive forces present, the $\bar{D}3$ -brane is expected to sit at the bottom of a throat. Here again, inflation takes place as the $D3$ -brane moves down the throat towards the $\bar{D}3$ -brane, with their separation distance as the inflaton, and inflation ends when they collide and annihilate each other, allowing the universe to settle down to the string vacuum state that describes

our universe today. Although the original version encounters some fine-tuning problems, the scenario becomes substantially better as we make it more realistic with the introduction of warped geometry [23].

Because of the warped geometry, a consequence of flux compactification, a mass M in the bulk becomes $h_A M$ at the bottom of a warped throat, where $h_A \ll 1$ is the warped factor (Figure 1). This warped geometry tends to flatten, by orders of magnitude, the inflaton potential $V(\phi)$, so the attractive $D3$ - $\bar{D}3$ -brane potential is rendered exponentially weak in the warped throat. The attractive gravitational (plus RR) potential together with the brane tensions takes the form

$$V(\phi) = 2T_3 h_A^4 \left(1 - \frac{1}{N_A} \frac{\phi_A^4}{\phi^4} \right) \quad (4.1)$$

where T_3 is the $D3$ -brane tension and the effective tension is warped to a very small value $T_3 h_A^4$. The warp factor h_A depends on the details of the throat. Crudely, $h(\phi) \sim \phi/\phi_{edge}$, where $\phi = \phi_{edge}$ when the $D3$ -brane is at the edge of the throat, so $h(\phi_{edge}) \simeq 1$. At the bottom of the throat, where $\phi = \phi_A \ll \phi_{edge}$, $h_A = h(\phi_A) = \phi_A/\phi_{edge}$. The potential is further warped because $N_A \gg 1$ is the $D3$ charge of the throat. The $D3$ - $\bar{D}3$ -brane pair annihilates at $\phi = \phi_A$. In terms of the potential (4.1), a tachyon appears as $\phi \rightarrow \phi_A$ so inflation ends as in hybrid inflation. The energy released by the brane pair annihilation heats up the universe to start the hot big bang. To fit data, $h_A \sim 10^{-2}$. If the last 60 e-folds of inflation takes place inside the throat, then $\phi_{edge} \geq \phi \geq \phi_A$ during this period of inflation. This simple model yields $n_s \simeq 0.97$, $r < 10^{-5}$ and vanishing non-Gaussianity.

The above model is very simple and well motivated. There are a number of interesting variations that one may consider. Within the inflaton potential, we can add new features to it. In general, we may expect an additional term in $V(\phi)$ of the form

$$\beta H^2 \phi^2 / 2$$

where H is the Hubble parameter so this interaction term behaves like a conformal coupling. Such a term can emerge in a number of different ways:

- Contributions from the Kähler potential and various interactions in the superpotential [23] as well as possible D-terms [24], so β may probe the structure of the flux compactification [25, 26].
- It can come from the finite temperature effect. Recall that finite temperature T induces a term of the form $T^2 \phi^2$ in finite temperature field theory. In de-Sitter universe, there is a Hawking-Gibbons temperature of order H thus inducing a term of the form $H^2 \phi^2$.
- The $D3$ -brane is attracted to the $\bar{D}3$ -brane because of the RR charge and the gravitational force. Since the compactified manifold has no boundary, the total RR charge inside must be zero, and so is the gravitational “charge”. A term of the above form

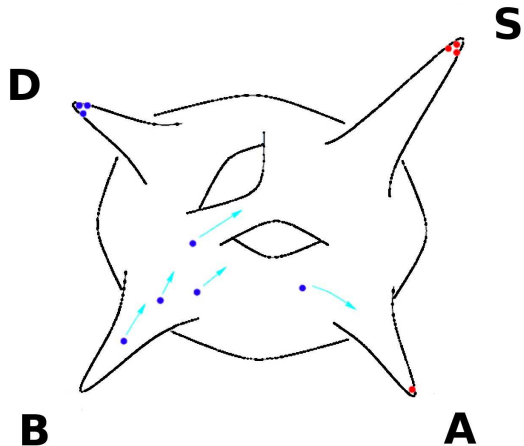


Figure 1: A pictorial sketch of a generic flux compactified 6-dimensional bulk, with a number of warped throats (4 of which are shown here). Besides the warped throats, there are $D7$ -branes wrapping 4-cycles. The blue dots stand for mobile $D3$ -branes while the red dots are $\bar{D}3$ -branes sitting at the bottoms of throats. In the $D3$ - $\bar{D}3$ -brane inflationary scenario, the tension of the brane pairs provide the vacuum energy that drives inflation as the $D3$ -brane moves down A-throat. Inflation ends as the $D3$ -brane annihilates with the $\bar{D}3$ -brane in A-throat. The standard model branes may live in A-throat or S-throat. As an alternative, inflation may take place while branes are moving out of B-throat.

appears if we introduce a smooth background “charge” to cancel the gravitational “charges” of the branes [27]. On the other hand, negative tension is introduced via orientifold planes in the brane world scenario. If the throat is far enough away from the orientifold planes, it is reasonable to ignore this effect.

Overall, β is a free parameter and so is naively expected to be of order unity, $\beta \sim 1$. However, the above potential yields enough inflation only if β is small enough, $\beta < 1/5$ [28]. The present PLANCK data implies that β is essentially zero or even slightly negative.

Another variation is to notice that the 6-dimensional throat can be quite non-trivial. In particular, if one treats the throat geometry as a Klebanov-Strassler deformed conifold, gauge-gravity duality leads to the expectation that ϕ will encounter steps as the $D3$ -brane moves down the throat [29]. Such steps, though small, may be observed in the CMB power spectrum.

Inflection Point Inflation

Since the 6-dimensional throat has one radial and 5 angular modes, $V(\phi)$ gets corrections that can have angular dependencies. As a result, its motion towards the bottom of the throat may follow a non-trivial path. One can easily imagine situation

where it will pass over an inflection point. Around the inflection point, $V(\phi)$ may take a generic simple form

$$V(\phi) \simeq V_0 + A\phi + B\phi^2/2 + C\phi^3/3$$

where $\eta = 0$ at the inflection point $B + 2C\phi = 0$. As shown in Ref.[26, 30], given that $V(\phi)$ is flat only around the inflection point, $N_e \sim 1/\sqrt{\epsilon}$, so ϵ must be very small, resulting in a very small r . Here $n_s - 1 = 2\eta$ so we expect n_s to be very close to unity, with a slight red or even blue tilt. Although motivated in brane inflation, an inflection point may be encountered in other scenarios of the inflationary universe, so it should not be considered as a stringy feature.

DBI Model

Instead of modifying the potential, string theory suggests that the kinetic term for a D -brane should take the Dirac-Born-Infeld form [31, 32]

$$\frac{1}{2}\partial^\mu\phi\partial_\mu\phi \rightarrow -\frac{1}{f(\phi)}\sqrt{1 - f(\phi)\partial^\mu\phi\partial_\mu\phi} + \frac{1}{f(\phi)} \quad (4.2)$$

where $f(\phi) \sim h(\phi)^{-4} \sim A/\phi^4$ is the warp factor of a throat. This DBI property is intrinsically a stringy feature. Here the warp factor plays the role of a brake that slows down the motion of the D -brane as it moves down the throat,

$$f(\phi)(\partial_t\phi)^2 < 1.$$

This braking mechanism is insensitive to the form of $V(\phi)$, so many e-folds is assured as $\phi \rightarrow 0$. It produces a negligibly small r but a large non-Gaussianity in the equilateral bi-spectrum as the sound speed becomes very small. The CMB data has an upper bound on the non-Gaussianity that clearly rules out the dominance of this stringy DBI effect. Nevertheless, it is a clear example that stringy features of inflationary scenarios may be tested directly by cosmological observation.

Instead of moving down a throat, one may also consider inflation while a brane is moving out of a throat [33, 34]. In this case, the predictions are not too different from that of the inflection point case.

$D3$ - $D7$ -brane Inflation

Here, the inflaton is the position of a $D3$ -brane moving relative to the position of a higher dimensional $D7$ -brane [35]. Since the presence of both $D3$ and $D7$ -branes preserves supersymmetry (as opposed to the presence of $D5$ -branes), inflation can be driven by a D-term and a potential of the form like

$$V(\phi) = V_0 + a \ln \phi - b\phi^2 + c\phi^4 + \dots$$

may be generated. Such a potential yields $n_s \simeq 0.98$, which may be a bit too big. One may lower the value a little by considering variations of the scenario. In any case, one ends up with a very small r .

4.2 Kähler Moduli Inflation

In flux compactification, the Kähler moduli are typically lighter than the complex structure moduli. Intuitively, this implies their effective potentials are flatter than those for the complex structure moduli. For a Swiss-cheese like compactification, besides the modulus for the overall volume, we can also have moduli describing the sizes of the holes inside the manifold. So it is reasonable to find situations where a Kähler modulus plays the role of the inflaton. A potential is typically generated by non-perturbative effects, so examples may take the form [36]

$$V \simeq V_0 (1 - Ae^{-k\phi}) \tag{4.3}$$

where both A and k are positive and of order unity or bigger. Here, $\eta \simeq -Ak^2e^{-k\phi} < 0$ and $\epsilon \simeq \eta^2/2k^2$, so the potential is very flat for large enough ϕ . If the inflaton measures the volume of a blow-up mode corresponding to the size of a 4-cycle in a Swiss-Cheese compactification in the large volume scenario, we have $k \sim \sqrt{\mathcal{V}} \ln \mathcal{V}$, where the compactification volume is of order $\mathcal{V} \sim 10^6$ in string units, so k is huge and $r \simeq 2(n_s - 1)^2/k^2 \sim 10^{-10}$. Models of this type are not close to saturating the Lyth bound (2.14). Other scenarios of this type again have very small r .

5. Large r Scenarios

The Lyth bound (2.14) implies that large r requires large inflaton field range $\Delta\phi \gg M_{Pl}$. A phenomenological model with relatively flat potential and large field range is not too hard to write down, e.g. chaotic inflation. However, the range of a typical modulus in string theory is limited by the size of compactification, $\Delta\phi < M_{Pl}$. Even if we could extend the field range (e.g. by considering an irregular shaped manifold), the corrections to a generic potential may grow large as ϕ explores a large range. Essentially, we lose control of the approximate description of the potential. Axions allow one to maintain control of the approximation used while exploring large ranges. Here we shall briefly review 2 ideas, namely the Kim-Nilles-Peloso Mechanism [37] and the axion monodromy [38, 39]. In both cases, an axion moves in a helical-like path. The flatness of the potential and the large field range appear naturally.

5.1 The Kim-Nilles-Peloso Mechanism

Let us start with a simple model and then build up to a model that is relatively satisfactory.

Natural Inflation

It was noticed long ago that axion fields may be ideal inflaton candidates because an axion field ϕ , a pseudo-scalar mode, has a shift symmetry, $\phi \rightarrow \phi + \text{constant}$. This symmetry is broken to a discrete symmetry by some non-perturbative effect so that a periodic potential is generated [18, 19],

$$V(\phi) = A \left(1 - \cos \left(\frac{\phi}{f} \right) \right) \rightarrow \frac{A}{2f^2} \phi^2 + \dots \sim \frac{m^2}{2} \phi^2 \quad (5.1)$$

where we have set the minima of the potential at $\phi = 0$ to zero vacuum energy. With suitable choice of A and f the resulting axion potential can be relatively small and flat, an important property for inflation. As f becomes large, this model approaches the (quadratic form) chaotic inflation [40], which is well studied. To have enough e-folds, we may need a large field range, say, $\Delta\phi > 14M_{Pl}$, which is possible here only if the decay constant $f > \Delta\phi \gg M_{Pl}$. This requires a certain degree of fine tuning since a typical f is expected to satisfy $f < M_{Pl}$ (see, for example, Fig. 2 in [41]). To fit the scalar mode perturbations of COBE $m \simeq 7 \times 10^{-6} M_{Pl}$. The range of predictions [41] in the r vs n_s plot is shown in Fig. 2.

N-flation

There are ways to get around this to generate enough e-folds. One example is to extend the model to include N different axions, each with a term of the form in Eq.(5.1), with a different decay constant $f_i < M_{Pl}$. This N-flation model [42] is a string theory inspired scenario since flux compactification results in the presence

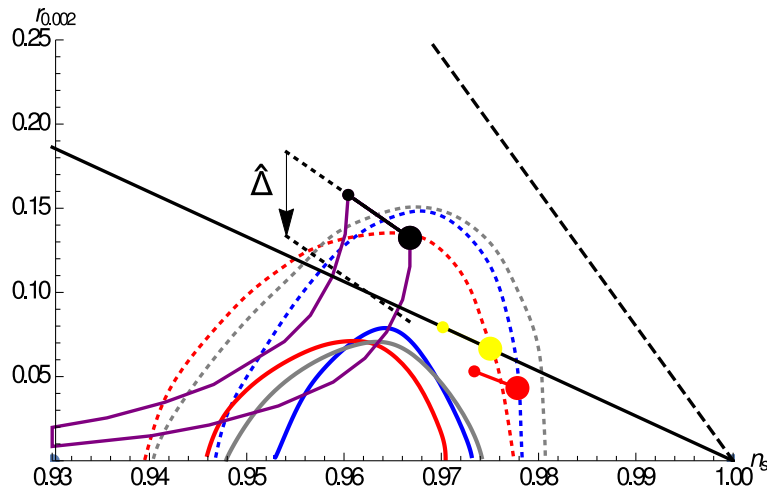


Figure 2: The tensor-to-scalar ratio r versus the primordial tilt n_s plot for pivot scale 0.002 Mpc^{-1} . Pairs of solid and dashed semi-circular lines encompass 68% and 95% confidence limits for r and n_s as given in Ref[10]. The regions are based on PLANCK data combined with: WMAP [large scale polarization] (grey), WMAP plus BAO [baryon acoustic oscillations in galaxy surveys] (blue), and WMAP plus higher ℓ CMB data [ACT and SPT] (red) as described in detail in Ref[10]. All remaining lines, points and arrows describe theoretical models. Convex potentials lie above the straight, solid black line; concave potentials below it. Power law inflation generates results along the straight, dashed line. String-related models include the short yellow segment for a linear inflaton potential $V \sim \phi$, the short red segment for $V \sim \phi^{2/3}$ and the short black segment (chaotic inflation) for $V \sim \phi^2$. Each small (large) dot stands for 50 (60) e-folds. Two purple lines moving to the left show the full range of predictions for natural inflation. All small field models and some large field ones suppress r (these are not plotted). The black arrow is the vertical shift $\hat{\Delta}$, illustrating how the results for *cosine* potential differ from those of the ϕ^2 potential.

of many axions. In the approximation that the axions are independent of each other (that is, their couplings with each other are negligible), the analysis is quite straightforward and interesting [43]. The predictions are similar to that of a large field model, that is, $0.93 < n_s < 0.95$ but $r \leq 10^{-3}$. In general, the axions do couple to each other and the situation can be quite complicated. For a particularly simple case, inspired by string theory and supergravity, a statistical analysis has been carried out and clear predictions can be made [43]. For a large number of axions, one has

$$V(\phi_i) = V_0 + \sum_i \alpha_i \cos\left(\frac{\phi_i}{f_i}\right) + \sum_{i,j} \beta_{ij} \cos\left(\frac{\phi_i}{f_i} - \frac{\phi_j}{f_j}\right). \quad (5.2)$$

The statistical distribution of results yields small values for r quite similar to that of the N-flation model.

Helical Inflation

Let us consider a particularly interesting case of a 2-axion model of the form [37]

$$V(\phi_1, \phi_2) = V_1 + V_2 = V_0 \left\{ 1 - \cos\left(\frac{\phi_1}{f_1}\right) + A \left[1 - \cos\left(\frac{\phi_1}{f_1'} - \frac{\phi_2}{f_2}\right) \right] \right\} \quad (5.3)$$

where we take $f_1' \ll f_1 \ll M_{Pl}$.

Note that the second term in V (5.3), namely V_2 , vanishes at

$$\frac{\phi_1}{f_1'} - \frac{\phi_2}{f_2} = 0. \quad (5.4)$$

This is the minimum of V_2 and the bottom of the trough of the potential V . For large enough A , inflaton will follow the trough as it rolls along its path. Now $\frac{f_1}{2\pi f_1'}$ measures the number of cycles that ϕ_2 can travel for $0 < \phi_1 < f_1$. Although ϕ_2 has a shift symmetry $\phi_2 \rightarrow \phi_2 + 2\pi f_2$, the path does not return to the same configuration after ϕ_2 has traveled for one period because ϕ_1 has also moved. Thus, instead of a shift symmetry, the system has a helical symmetry. Moving along the path of the trough (5.4), we see that the second term in the potential (5.3) vanishes and so the potential V reduces to that with only the first term and the range of the inflaton field ϕ_2 can easily be super-Planckian.

To properly normalize the fields, one defines two normalized orthogonal directions,

$$X = \frac{f_1'\phi_1 + f_2\phi_2}{\sqrt{f_1'^2 + f_2^2}}, \quad Y = \frac{f_2\phi_1 - f_1'\phi_2}{\sqrt{f_1'^2 + f_2^2}}, \quad (5.5)$$

the inflaton will roll along the X -direction while Y -direction is a heavy mode which can be integrated out. Note that the system is insensitive to the magnitude of A as long as it is greater than $\mathcal{O}(1)$ such that Y -direction is heavy enough. For instance, the slow roll parameters ϵ and η are not affected which means that the observables n_s and r are insensitive to A . Since the X path is already at the minimum of the second term, at $Y = 0$, the effective potential along X is determined by V_1 ,

$$V(X) = V_0 \{1 - \cos(X \cos \theta / f_1)\} \approx \frac{1}{2} \frac{V_0 X^2}{f_1^2} \cos^2 \theta \quad (5.6)$$

$$\cos \theta \equiv \frac{f_1'}{\sqrt{f_1'^2 + f_2^2}}. \quad (5.7)$$

So this helical model is reduced to the single *cosine* model (5.1) where

$$f = (f_1/f_1') \sqrt{f_1'^2 + f_2^2} \simeq f_1 f_2 / f_1'$$

can be bigger than M_{Pl} even if all the individual $f_i < M_{Pl}$.

So it is not difficult to come up with stringy models that can fit the existing data. In view of the large B-mode reported by BICEP2 [6], this model was revisited

by a number of groups [44, 45, 46, 47, 48, 49, 50, 51]. In fact, one can consider a more general form for $V_1(\phi_1)$ [52], which can lead to a large field range model with somewhat different predictions.

Since the shift symmetry of an axion is typically broken down to some discrete symmetry, the above *cosine* model is quite natural. The generalization to more than 2 axions is straightforward, and one can pile additional helical motions on top of this one, increasing the value of the effective decay constant f by additional big factors. All models in this class reduce to a model with a single *cosine* potential, which in turn resembles the quadratic version of chaotic inflation. This limiting behavior is quite natural in a large class of axionic models in the supergravity framework [53]. Because of the periodic nature of an axionic potential, this *cosine* model can have a smaller value of r than chaotic inflation [40]. The deviations from chaotic inflation occur in a well-defined fashion. Let

$$\hat{\Delta} = 16\Delta = r + 4(n_s - 1) = -4M_{Pl}^2/f^2 \quad (5.8)$$

where ϕ^2 chaotic inflation has $\hat{\Delta} = 0$ while the *cosine* model has $\hat{\Delta} < 0$. All other quantities such as runnings of spectral indices have very simple dependencies on $\hat{\Delta}$. As shown in Table 1, this deviation is quite distinctive of the periodic nature of the inflaton potential. For $n_s = 0.96$, $r = 0.16$ in the ϕ^2 model, while r can be as small as $r = 0.04$ (or $\hat{\Delta} = -0.12$) in the *cosine* model. As data improves, a negative value of $\hat{\Delta}$ can provide a distinctive signature for a periodic axionic potential for inflation.

$V(\phi)$	$\frac{1}{2}m^2\phi^2$	$V_0 \left[1 - \cos\left(\frac{\phi}{f}\right) \right]$
$\epsilon = \frac{1}{2}(V'/V)^2$	$\frac{1}{16}r$	$\frac{1}{16}r$
$\eta = V''/V$	$\frac{1}{16}r$	$\frac{1}{16}r + 2\Delta$
$\xi^2 = V'V'''/V^2$	0	$\frac{1}{2}r\Delta$
$\omega^3 = V'^2V''''/V^3$	0	$\frac{1}{32}r^2\Delta + r\Delta^2$
$n_s - 1 = 2\eta - 6\epsilon$	$-\frac{1}{4}r$	$-\frac{1}{4}r + 4\Delta$
$n_t = -2\epsilon$	$-\frac{1}{8}r$	$-\frac{1}{8}r$
$\frac{dn_s}{d\ln k} = -16\epsilon\eta + 24\epsilon^2 + 2\xi^2$	$\frac{1}{32}r^2$	$\frac{1}{32}r^2 - r\Delta$
$\frac{dn_t}{d\ln k} = -4\epsilon\eta + 8\epsilon^2$	$\frac{1}{64}r^2$	$\frac{1}{64}r^2 - \frac{1}{2}r\Delta$
$\frac{d^2n_s}{d\ln k^2} = -192\epsilon^3 + 192\epsilon^2\eta - 32\epsilon\eta^2 - 24\epsilon\xi^2 + 2\eta\xi^2 + 2\omega^3$	$-\frac{1}{128}r^3$	$-\frac{1}{128}r^3 + \frac{3}{8}r^2\Delta - 4r\Delta^2$

TABLE 1, Comparison between ϕ^2 chaotic inflation and the *cosine* model for the various physically measurable quantities [45] where Δ (5.8) measures the difference. Here $M_{Pl} = 1$.

5.2 Axion Monodromy

The above idea of extending the effective axion range can be carried out with a single axion, where the axion itself executes a helical motion. This is the axion

monodromy model [38, 39]. In this scenario, inflation can persist through many periods around the configuration space, thus generating an effectively large field range with an observable r .

Recall that a gauge field, or one-form field (i.e., with one space-time index), is sourced by charged point-like fields, while a 2-form (anti-symmetric tensor) field is sourced by strings. So we see that there will be at least one 2-form field in string theory. Consider a 5-brane that fills our 4-dimensional space-time and wraps a 2-cycle inside the compactified manifold. The axion is the integral of a 2-form field over the 2-cycle. Integrating over this 2-cycle, the 6-dimensional brane action produces a potential for the axion field in the resulting 4-dimensional effective theory. Here, the presence of the brane breaks the axion shift symmetry and generates a monodromy for the axion. For NS5-branes, a typical form of the axion potential (coming from the DBI action) is

$$V(\phi) = A\sqrt{b^2 + \phi^2}. \quad (5.9)$$

For small parameter b , $V(\phi) \simeq A\phi$. The prediction of such a linear potential is shown in Fig. 2. One can consider $D5$ -branes instead. $D7$ -branes wrapping 4-cycles in the compactified manifold is another possibility. For large values of ϕ , a good axion monodromy model requires that there is no uncontrollable higher order stringy or quantum corrections that would spoil the above interesting properties [54, 55, 56]. Variants of this picture may allow a more general form of the potential, say $V(\phi) \sim \phi^p$ where p can take values such as $p = 2/3, 4/3, 2, 3$, thus generating $r \simeq 0.04, 0.09, 0.13$ and 0.2 , respectively. The $p = 2$ case predicts a n_s value closest to $r \sim 0.16$ reported by BICEP2 after accounting for dust. The observational bounds are currently under scrutiny. Readers are referred to Ref[4] for more details.

5.3 Discussions

If BICEP2's detection of r is confirmed, it does not necessarily invalidate completely all the small r models discussed above. It may be possible to modify some of them to generate a large enough r . As an example, if one is willing to embed the $D3$ - $\bar{D}3$ -brane inflation into a warm inflationary model, a $r \simeq 0.2$ may be viable [57]. It will be interesting to re-examine all the small r string theory models and see whether and how any of them may be modified to produce a large r .

As string theory has numerous solutions, it is not surprising that there are multiple ways to realize the inflationary universe scenario. With cosmological data available today, theoretical predictions and contact with observations are so far quite limited. As a consequence, it is rather difficult to distinguish many string theory inspired predictions from those coming from ordinary field theory (or even supergravity models). There are exceptions, as pointed out earlier. For example, the DBI inflation prediction of an equilateral bi-spectrum in the non-Gaussianity, or the determined spacing of steps in the power spectrum itself, may be considered to be

distinct enough that if either one is observed, some of us may be convinced that it is a smoking gun of string theory. Although searches for these phenomena should and would continue, so far, we have not been lucky enough to see any hint of them.

Here we like to emphasize that there is another plausible signature to search for. Since all fundamental objects are made of superstrings (we include $D1$ -strings here), and the universe is reheated to produce a hot big bang after inflation, it is likely that, besides strings in their lowest modes which appear as ordinary particles, some relatively long strings will also be produced, either via the Kibble mechanism or some other mechanism. They will appear as cosmic strings.

When there are many axions, or axion-like fields, with a variety of plausible potentials, the possibilities may be quite numerous and so predictions may be somewhat imprecise. For any axion or would-be-Goldstone bosons, with a continuous $U(1)$ symmetry, we expect a string-like defect which can end up as cosmic strings if generated in early universe. In field theory, a vortex simply follows from the Higgs mechanism where the axion a appears as the phase of a complex scalar field, $\Phi = \rho e^{ia/f}$. In string theory, we note that such an axion a is dual to a 2-form tensor field $C_{\lambda\kappa}$, i.e., $\partial^\mu a = \epsilon^{\mu\nu\lambda\kappa} \partial_\nu C_{\lambda\kappa}$. As pointed out earlier, such a 2-form field is sourced by a string. So the presence of axions would easily lead to cosmic strings (i.e., vortices, fundamental strings and $D1$ -strings) and these may provide signatures of string theory scenarios for the inflationary universe. This is especially relevant if cosmic strings come in a variety of types with different tensions and maybe even with junctions.

Following Fig. 1, we see that besides the axions responsible for inflation, there may be other axions. Some of them may have mass scales warped to very small values. If a potential of the form (5.1) is generated, a closed string loop becomes the boundary of a domain wall, or membrane. It will be interesting to study the effect of the membrane on the evolution of a cosmic string loop. The tension of the membrane and the axion mass are of order

$$\sigma \sim \sqrt{A}f, \quad m^2 = A/f^2$$

It is interesting to entertain the possibility that this axion can contribute substantially to the dark matter of the universe. If so, its contribution to the energy density is roughly given by A while its mass is estimated to be $m \simeq 10^{-22}$ eV [58]. This yields $A \simeq 10^{-118} M_{Pl}^4$, $f \simeq \sqrt{A}/m \simeq 10^{-10} M_{Pl}$ and $\sigma \simeq 10^{-69} M_{Pl}^3 \simeq 10^{-14}$ GeV³. For such a small membrane tension, the evolution of the corresponding cosmic string is probably not much changed.

6. Relics: Low Tension Cosmic Strings

Witten's [59] original consideration of macroscopic cosmic strings was highly influential. He argued that the fundamental strings in heterotic string theory had tensions too large to be consistent with the isotropy of the COBE observations. Had they been produced they would be inflated away. It is not even clear how inflation might be realized within the heterotic string theory.

However, with the discovery of D -branes [60], the introduction of warped geometries [61] and the development of specific, string-based inflationary scenarios, the picture has changed substantially. Open fundamental strings must end on branes; so both open and closed strings are present in the brane world. Closed string loops inside a brane will break up into pieces of open strings, so only vortices (which may be only meta-stable) can survive inside branes. Here, $D1$ -strings (i.e., $D1$ -branes) may be treated as vortices inside branes and survive long enough to be cosmologically interesting [62].

The warped geometry will gravitationally redshift the string tensions to low values and, consequently, strings can be produced *after* inflation. A string with tension T in the bulk will be warped to $\mu = h^2 T$ with h being the warp factor, which can be very small when the string is sitting at the bottom of a throat. (It is $h = h_A$ in Eq.(4.1) in throat A.) That is important because relics produced during inflation are rapidly diluted by expansion. Only those generated after (or very near the end of) inflation are potentially found within the visible universe. Since the Type IIB model has neither $D0$ -branes nor $D2$ -branes, the well-justified conclusion that our universe is dominated neither by monopoles nor by domain walls follows automatically. Scenarios that incorporate string-like relics may prove to be consistent with all observations. Such relics appear to be natural outcomes of today's best understood string theory scenarios.

The physical details of the strings in Type IIB model can be quite non-trivial, including the types of different species present and the range of string tensions. Away from the branes, p fundamental F1-strings and q $D1$ -strings can form a (p, q) bound state, with a (p, q) string tension [63]. Junctions of strings will be present automatically. If they live at the bottom of a throat, there can be beads at the junctions as well [64]. Finally, there is some evidence that strings can move in both internal and external dimensions and are not necessarily confined to the tips of the throat [65]. This behavior can show up as a cosmic string with variable tension.

As we will describe in more detail, all indications suggest that, once produced after inflation, a scaling cosmic string network will emerge for the stable strings. Before string theory's application to cosmology, the typical cosmic string tension was presumed to be set by the grand unified theory's (GUTs) energy scale. Such strings have been ruled out by observations. We will review the current limits shortly. Warped geometry typically allows strings with tensions that are substantially smaller,

avoiding the observational constraints on the one hand and frustrating easy detection on the other. The universe's expansion inevitably generates sub-horizon string loops and if the tension is small enough the loops will survive so long that their peculiar motions are damped and they will cluster in the manner of cold dark matter. This results in a huge enhancement of cosmic string loops within our galaxy (about 10^5 times larger at the Sun's position than the mean throughout the universe) and makes detection of the local population a realistic experimental goal in the near future. We will focus on the path to detection by means of microlensing. Elsewhere, we will discuss blind, gravitational wave searches.

A microlensing detection will be very distinctive. The nature of a microlensing loop can be further confirmed and studied through its unique gravitational wave signature involving emission of multiple harmonics of the fundamental loop period from the precise microlensing direction. Since these loops are essentially the same type of string that makes up all forms of microscopic matter in the universe, their detection will be of fundamental importance in our understanding of nature.

6.1 Strings in Brane World Cosmology

String-like defects or fundamental strings are expected whenever reheating produces some closed strings towards the end of an inflationary epoch. Once inflation ends and the radiation dominated epoch begins, ever larger sections of this cosmic string network re-enter the horizon. The strings move at relativistic speeds and long lengths collide and break off sub-horizon loops. Loops shrink and evaporate by emitting gravitational waves in a characteristic time $\tau = l/(\Gamma G\mu)$ where l is the invariant loop size, μ is the string tension while Γ is numerically determined and $\Gamma \sim 50$ for strings coupled only to gravity [5]. To ease discussion, we shall adopt this value for Γ .

String tension is the primary parameter that controls the cosmic string network evolution, first explored in the context of phase transitions in grand unified field theories (GUTs), which may be tied to the string scale. Assuming that the inflation scale is comparable to the GUT scale, inflation generated horizon-crossing defects whose tension is set by the characteristic grand unification energy [5]. These GUT strings with $G\mu \sim 10^{-6}$ would have seeded the density fluctuations for galaxies and clusters but have long been ruled out by observations of the cosmic microwave background (CMB) [9, 66, 67].

Here, string theory comes to the rescue. Six of the string theory's 9 spatial dimensions are stably compactified. The flux compactification involves manifolds possessing warped throat-like structures which redshift all characteristic energy scales compared to those in the bulk space. In this context, cosmic strings produced after inflation living in or near the bottoms of the throats can have different small tensions [68, 69, 70, 71, 72]. The quantum theory of one-dimensional objects includes a host of *effectively* one-dimensional objects collectively referred to here as superstrings. For

example, a single $D3$ -brane has a $U(1)$ symmetry that is expected to be broken, thus generating a string-like defect. (For a stack of n branes, the $U(n) \supset U(1)$ symmetry is generic.) Note that fundamental superstring loops can exist only away from branes. Any superstring we observe will have tension μ exponentially diminished from that of the Planck scale by virtue of its location at the bottom of the throat. Values like $G\mu < 10^{-14}$ (i.e. energies $< 10^{12}$ GeV) are entirely possible. A typical manifold will have many throats and we expect a distribution of μ , presumably with some $G\mu > 10^{-14}$.

In addition to their reduced tensions, superstrings should differ from standard field theory strings (i.e., vortices) in other important ways: long-lived excited states with junctions and beads may exist, multiple non-interacting species of superstrings may coexist and, finally, the probability for breaking and rejoining colliding segments (intercommutation) can be much smaller than unity [73]. Furthermore a closed string loop may move inside the compacted volume as well. Because of the warped geometry there, such motion may be observed as a variable string tension both along the string length and in time.

6.2 Current Bounds on String Tension $G\mu$ and Probability of Intercommutation p

Empirical upper bounds on $G\mu$ have been derived from null results for experiments involving lensing [74, 75, 76, 77, 78, 79, 80, 81, 82], gravitational wave background and bursts [83, 84, 85, 86, 87, 88, 89, 90, 91, 92, 93, 94, 95, 96], pulsar timing [97, 75, 98, 99, 100, 101, 102] and cosmic microwave background radiation [9, 66, 103, 104, 105, 106, 107, 108, 67, 109, 110, 111, 112, 113, 114, 10, 115]. We will briefly review some recent results but see [116, 117] for more comprehensive treatments.

All bounds on string tension depend upon uncertain aspects of string physics and of network modeling. The most important factors include:

- The range of loop sizes generated by network evolution. “Large” means comparable to the Hubble scale, “small” can be as small as the core width of the string. Large loops take longer to evaporate by emission of gravitational radiation.
- The probability of intercommutation p is the probability that two crossing strings break and reconnect to form new continuous segments. Field theory strings have $p \sim 1$ but superstrings may have p as small as 10^{-3} . The effect of lowering p is to increase the network density of strings to maintain scaling.
- The physical structure of the strings. F1 strings are one-dimensional, obeying Nambu-Goto equations of motion. $D1$ strings and field theory strings are vortices with finite cores.

- The mathematical description of string dynamics used in simulations and calculations. The Abelian Higgs model is the simplest vortex description but the core size in calculations is not set to realistic physical values. Abelian Higgs and Nambu-Goto descriptions yield different string dynamics on small scales.
- The number of stable string species. Superstring have more possibilities than simple field theory strings. These include bound states of F1 and $D1$ strings with beads at the junctions and non-interacting strings from different warped throats.
- The charges and/or fluxes carried by the string. Many effectively one-dimensional objects in string theory can experience non-gravitational interactions.
- The character of the discontinuities on a typical loop. The number of cusps and/or the number of kinks governs the emitted gravitational wave spectrum.

While there has been tremendous progress, all of these areas are under active study.

When the model-related theoretical factors are fixed each astrophysical experiment probes a subset of the string content of spacetime. For example, CMB power spectrum fits rely on well-established gross properties of large-scale string networks which are relatively secure but do not probe small sized loops which may dominate the total energy density and which would show up only at large ℓ . Analysis of combined PLANCK, WMAP, SPT and ACT data [115] implies $G\mu < 1.3 \times 10^{-7}$ for Nambu-Goto strings and $G\mu < 3.0 \times 10^{-7}$ for field theory strings. Limits from optical lensing in fields of background galaxies rely on the theoretically well-understood deficit angle geometry of a string in spacetime but require a precise accounting for observational selection effects. Analysis of the GOODS and COSMOS optical surveys [81, 82] yields $G\mu < 3 \times 10^{-7}$. Taken together these observations imply $G\mu \lesssim 1-3 \times 10^{-7}$.

There is a well-established bound on the gravitational energy density at the time of Big Bang Nucleosynthesis because an altered expansion rate impacts light element yields (e.g. [118]). The gravitational radiation generated by any string network cannot exceed the bounds. If a network forms large Nambu-Goto loops of one type of string with intercommutation probability p an estimate of the BBN constraint [119] is $G\mu \lesssim 5 \times 10^{-7} p^2$ (this depends implicitly on the loop formation size and a still-emerging understanding of how network densities vary with p). LIGO's experimental bound on the stochastic background gravitational radiation [95] from a similar network implies a limit on $G\mu$ of the same general form as the BBN limit but weaker. Advanced LIGO is projected to reach $G\mu \sim 10^{-12}$ for $p = 1$ [119]. The same LIGO results can be used to place a reliable, conservative bound of $G\mu < 2.6 \times 10^{-4}$ over a much wider range of possible models, almost independent of loop size and of frequency scaling of the emission [117].

More stringent bounds rely on additional assumptions. Consider a specific set of choices for the secondary parameters of strings: one string species, Nambu-Goto

dynamics, only gravitational interactions, large loops ($\alpha = 0.1$), each with a cusp. The time of arrival of pulses emitted by a pulsar vary on account of the gravitational wave background. When the sequence is observed to be regular the perturbing amplitude of the waves is limited. The current limit is $G\mu \lesssim 10^{-9}$ for $p = 1$ and $\lesssim 10^{-12}$ for $p = 10^{-3}$ [102]. Figure 3 is a graphical summary that illustrates some of the bounds discussed. The BBN (orange line) and CMB (yellow line) constraints are shown as a function of string tension $G\mu$ and intercommutation probability p . The Parkes Pulsar Timing Array limit (blue line) [100] and the NANOGrav limit (red dotted line) [102] are based on radiating cusp models. Each constraint rules out the area below and to the right of a line. Most analyses do not account for the fact that only a small fraction of horizon-crossing string actually form large loops which are ultimately responsible for variation in arrival times. In this sense the lines may be over-optimistic (see figure caption).

Superconducting strings have also been proposed [120]. The bound on superconducting cosmic strings is about $G\mu \lesssim 10^{-10}$ [121]. Interestingly, it was pointed out that the recently observed fast radio bursts can be consistent with being produced by superconducting cosmic strings [122].

In short, cosmic superstrings are generically produced towards the end of inflation and observations imply tensions substantially less than the original GUT-inspired strings. Multiple, overlapping approaches are needed to minimize physical uncertainties and model-dependent aspects. There is no known theoretical impediment to the magnitude of $G\mu$ being either comparable to or much lower than the current observational upper limits.

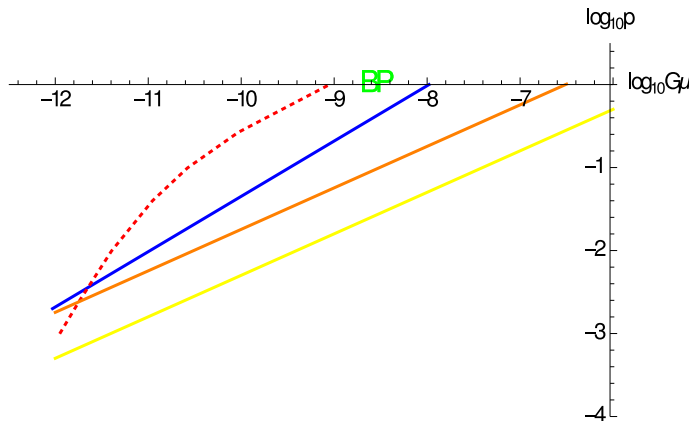


Figure 3: Observational constraints limit string tension and intercommutation probability if the network forms large loops. Each line is a particular observational constraint. The region below and to the right of a line is disfavored. Smaller p increases the number density of loops and larger $G\mu$ increases gravitational signal amplitude. Conversely, the region to the left and above a line remains consistent with observational limits. The illustrated constraints are: Big Bang Nucleosynthesis (orange line) and CMB (yellow line) from the gravitational wave spectra in [119], pulsar time of arrival for the Parkes Pulsar Timing Array (blue line, based on the analytic form in [100]) and for NANOGrav (red dotted line) in [102]. All lines depend upon theoretical modeling of the network, especially the fraction of large loops formed. For example, the initials BP (green) [123] are an example in which this fraction has been inferred from simulations and the bound on $G\mu$ at $p = 1$ indicated (the line has not been calculated). This result is approximately ~ 30 times *less* restrictive on $G\mu$ than an equivalent analysis in which all loops are born at a single large size as has been assumed in all the other analyses.

7. Scaling, Slowing, Clustering and Evaporating

The important physical processes are network scaling and loop slowing, clustering and evaporating.¹ Simulated cosmological string networks converge to self-similar scaling solutions [5, 73, 105]. Consequently Ω_{long} (Ω_{loop}), the fraction of the critical density contributed by horizon-crossing strings (loops), is independent of time while the characteristic size of a loop formed at time t scales with the size of the horizon: $l = \alpha t$ for some fixed α . To achieve scaling, long strings that enter the horizon must be chopped into loops sufficiently rapidly – if not, the density of long strings increases and over-closes the universe. In addition, loops must be removed so that Ω_{loop} stabilizes – if not, loops would come to dominate the contribution of normal matter. Scaling of the string network is an attractor solution in many well-studied models and the universe escapes the jaws of both Scylla and Charybdis. The inter-

¹Material in this section [124].

commutation probability determines the efficiency of chopping and μ determines the rate of loop evaporation.

Studies of GUT strings [5] took $G\mu \sim 10^{-6}$ (large enough to generate perturbations of interest at equipartition) and α small (set by early estimates of gravitational wave damping on the long strings) with the consequence $H\tau \sim \alpha/\Gamma G\mu \ll 1$ where H is the Hubble constant. Newly formed GUT loops decay quickly. The superstrings of interest here have smaller $G\mu$ so that loops of a given size live longer. In addition, recent simulations [125, 126, 127, 128, 129] produce a range of large loops: $10^{-4} \lesssim \alpha \lesssim 0.25$. The best current understanding is that $\sim 10 - 20\%$ of the long string length that is cut up goes into loops comparable to the scale of the horizon ($\alpha \sim 0.1$) while the remaining $\sim 80 - 90\%$ fragments to much smaller size scales [130, 131]. The newly formed, large loops are the most important contribution for determining today's loop population.

Cosmic expansion strongly damps the initial relativistic center of mass motions of the loops and promotes clustering of the loops as matter perturbations grow [132, 133]. Clustering was irrelevant for the GUT-inspired loops. They moved rapidly at birth, damped briefly by cosmic expansion and were re-accelerated to mildly relativistic velocities by the momentum recoil of anisotropic gravitational wave emission (the rocket effect) before fully evaporating [134, 135, 84]. GUT loops were homogeneously distributed throughout space. By contrast, below a critical tension $G\mu \sim 10^{-9}$ all superstring loops accrete along with the cold dark matter [133].

Loops of size $l = l_g \equiv \Gamma G\mu t_0$ are just now evaporating where t_0 is the age of the universe. The mean number density of such loops is dominated by network fragmentation when the universe was most dense, i.e. at early times. When they were born they came from the large end of the size spectrum, i.e. a substantial fraction of the scale of the horizon. The epoch of birth is $t_i = l_g/\alpha = \Gamma G\mu t_0/\alpha$. For $G\mu < 7 \times 10^{-9}(\alpha/0.1)(50/\Gamma)$ loops are born before equipartition in Λ CDM, i.e. $t_i < t_{eq}$. The smallest loops today have $l_g \approx 40\text{pc}(G\mu/2 \times 10^{-10})$ with characteristic mass scale $M_g = 1.7 \times 10^5 M_\odot (G\mu/2 \times 10^{-10})^2$ for $\Gamma = 50$.

Loop number and energy densities today are dominated by the scale of the gravitational cutoff, the smallest loops that have not yet evaporated. The characteristic number density $dn/d \log l \propto (\Gamma G\mu)^{-3/2} (\alpha t_{eq}/t_0)^{1/2} / t_0^3$ and the energy density $d\rho_{loop}/d \log l \sim \Gamma G\mu t_0 dn/d \log l$. The latter implies $\Omega_{loops} \propto \sqrt{\alpha G\mu/\Gamma}$ whereas $\Omega_{long} \propto \Gamma G\mu$. In scenarios with small μ it's the loops that dominate long, horizon-crossing strings in various observable contexts. The probability and rate of local lensing are proportional to the energy density.

Loops are accreted as the galaxy forms. Figure 4 illustrates schematically the constraints for a loop with typical initial peculiar velocity to be captured during galaxy formation and to remain bound today. The loop must lie within the inner triangular region which delimits small enough tension and early enough time of formation. Above the horizontal line capture is impossible; below the diagonal line

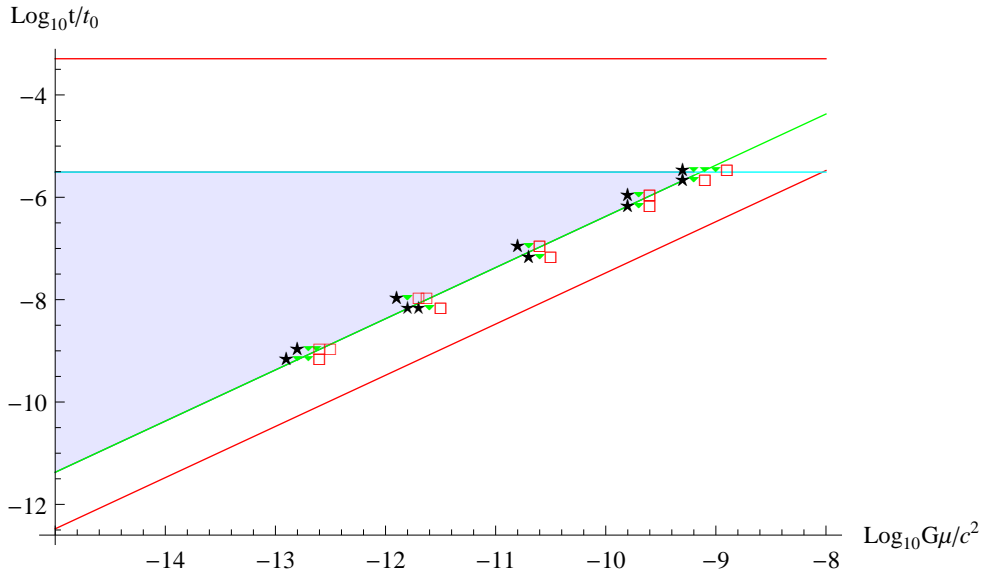


Figure 4: Bounds on formation time and string tension for a loop with initial velocity $v_i = 0.1$ to be captured at physical radius 30 kpc by galaxy formation. **(1)** Upper bounds on the formation time t_i/t_0 are given by the horizontal lines. The condition that cosmic drag lower the velocity to less than the circular rotation velocity today is given by the red line. The more stringent condition that capture occur at 30 kpc is given by the turquoise line. **(2)** Upper bounds on the string tension $G\mu$ are given by the diagonal lines. The condition that the loop be younger than its gravitational wave decay timescale is given by the red line. The more stringent condition that the loop not be accelerated out of the galaxy by today is given by the green line. **(3)** The shaded region encompasses string tensions and formation times giving bound loops at 30 kpc for $v_i = 0.1$ and $\alpha = 0.1$. The critical value of $G\mu$ below which clustering is possible is determined by the upper right hand corner of the green and turquoise lines. Lowering v_i raises the limit on t_i/t_0 (horizontal lines moves upward); lowering α shifts the bound to smaller $G\mu$ (diagonal lines moves leftward). Shifting the loop orbital scale to smaller values (say the solar position) requires earlier formation times (horizontal lines shifts down) and allows larger $G\mu$ (green line shifts to the right but is limited by the red line which is fixed). **(4)** The geometric symbols illustrate the sensitivity of the rocket effect. These are numerical experiments examining the outcome today ($t = t_0$) for groups of 10-20 loops captured at 30 kpc with slightly different string tensions: stars = all loops bound, boxes = all loops ejected, triangles = some bound and some ejected (for clarity the points are slightly offset in the vertical but not the horizontal direction).

detachment by the rocket effect has already occurred. The critical tension for loop clustering in the galaxy is set by the right hand corner of the allowed region.

To briefly summarize: \mathcal{F} , the enhancement of the galactic loop number density over the homogeneous mean, simply traces \mathcal{E} , the enhancement of cold dark matter over $\Omega_{DM}\rho_c$, for critical density ρ_c . This encapsulates conclusions of a study of the

growth of a galactic matter perturbation and the simultaneous capture and escape of network-generated loops [133]. At a typical galactocentric distance of 11 kpc $\log_{10} \bar{\mathcal{F}} = \log_{10} \bar{\mathcal{E}} + f(y)$ where $\log_{10} \bar{\mathcal{E}} = 5.5$ and $f(y) = -0.337 - 0.064y^2 - g(y)$ and $g(y) = 5(1 + \tanh(y - 7))$. The tension-dependent deviation from loops as passive tracers of cold dark matter is $f(y)$, $y = \log_{10}(G\mu/10^{-15})$, fit for $0 \leq y \leq 5$ from the capture study. Clustering saturates for small tensions: $f(y) = f(0)$ for $y < 0$. The over-bar indicates quantities averaged over the spherical volume and, in the case of the loops, a weighting by loop length in the capture study.

The extra piece $g(y)$ plays a role for $G\mu > 10^{-10}$ where it describes the suppression in clustering as one approaches the upper right corner of the triangle in figure 4. Numerical simulations have not yet accurately determined it.

A single $f(y)$ fits a range of radii as long as $\bar{\mathcal{E}} \gg 1$ (typically, galactic distances less than ~ 100 kpc). So we can easily have an enhancement $\mathcal{F} \sim 10^5$ for $G\mu \sim 10^{-14}$ at the Sun’s position. By comparison, GUT loops would have $\mathcal{F} = 1$ for all positions and tensions.

The model accounts for the local population of strings and we have used it to estimate microlensing rates, and LISA-like, LIGO-like and NANOGrav-like burst rates.

7.1 Large-scale String Distribution

We will start with a “baseline” description (loops from a network of a single, gravitationally interacting, Nambu-Goto string species with reconnection probability $p = 1$). The detailed description [133] was motivated by analytic arguments [130, 131] that roughly 80% of the network invariant length was chopped into strings with very small loop size ($\alpha \sim G\mu$) and by the numerical result [125, 126, 127, 128, 129] that the remaining 20% formed large, long-lived loops ($\alpha = 0.1$). At a given epoch loops are created with a range of sizes but only the “large” ones are of interest for the local population. The baseline description is supposed to be directly comparable to numerical simulations which generally take $p = 1$. The most recent simulations [123] are qualitatively consistent.

Next, we parameterize the actual “homogeneous” distribution in the universe when string theory introduces a multiplicity of string species and the reconnection probability p may be less than 1. And finally we will form the “local” distribution which accounts for the clustering of the homogeneous distribution.

In a physical volume V with a network of long, horizon-crossing strings of tension μ with persistence length L there are V/L^3 segments of length L . The physical energy density is $\rho_\infty = \mu L/V = \mu/L^2$. The persistence length evolves as the universe expands. A scaling solution demands $L \propto t$ during power law phases. There are also loops within the horizon; their energy is not included in ρ_∞ and the aim of the model is to infer the number density of loops of a given invariant size.

Kibble [136] developed a model for the network evolution for the long strings and loops in cosmology. It accounted for the stretching of strings and collisional intercommutation (long string segments that break off and form loops; loops that reconnect to long string segments). A variety of models of differing degrees of realism have been studied since then, guided by ever more realistic numerical simulations of the network. As a simple approximate description we focus on the Velocity One Scale model [137] in a recently elaborated form [138, 139]. The reattachment of loops to the network turns out to be a rather small effect and is ignored. We extended existing treatments by numerically evaluating the total loop creation rate in flat Λ CDM cosmology. The loop energy in a comoving volume varies like $\dot{E}_l = C\rho_\infty pva^3/L$ where C is the chopping efficiency, p is the intercommutation probability and v is the string velocity. All quantities on the right hand side except p vary in time; C is a parameterized fit in matter and radiation eras.

By integrating the model from large redshift to the current epoch one evaluates the fraction of the network that is lost to loop formation. The rate at which the loop energy changes is $\dot{E}_l = \mathcal{A}\mu a^3/(p^2t^3)$ where \mathcal{A} is a slowly varying function of redshift z and p shown in Figure 5. The plotted variation of \mathcal{A} with redshift indicates departures from a pure scaling solution (consequences of the radiation to matter transition for $a(t)$ and the implicit variation of chopping efficiency C). Knowing \mathcal{A} as a function of redshift and p is the input needed to evaluate of the loop formation rate. Loops form with a range of sizes at each epoch. Parameterize the size at the time of formation as αt . A very important feature predicted by theoretical analyses is that a large fraction of the invariant length goes into loops with $\alpha \sim G\mu$ or smaller. The limiting behavior of numerical simulations as larger and larger spacetime volumes are modeled suggests $\sim 80\%$ of the chopped up long string bears that fate. Such loops evaporate rapidly without contributing to the long-lived local loop population. The remaining 20% goes into large loops with $\alpha \sim 0.1$. Parameterize this fraction as $f = 0.2$. The birth rate density for loops born with size αt_b is

$$\left(\frac{dn}{dt dl}\right) = \frac{f\mathcal{A}}{\alpha p^2 t_b^4} \delta(l - \alpha t_b) \quad (7.1)$$

A loop formed at t_b with length l_b shrinks by gravitational wave emission. Its size is

$$l = l_b - \Gamma G\mu(t - t_b) \quad (7.2)$$

at time t ($\Gamma \sim 50$).

The number density of loops of size l at time t is the integral of the birth rate density over loops of all length created in the past. For $l < \alpha t$ or, equivalently, $t_b < t$

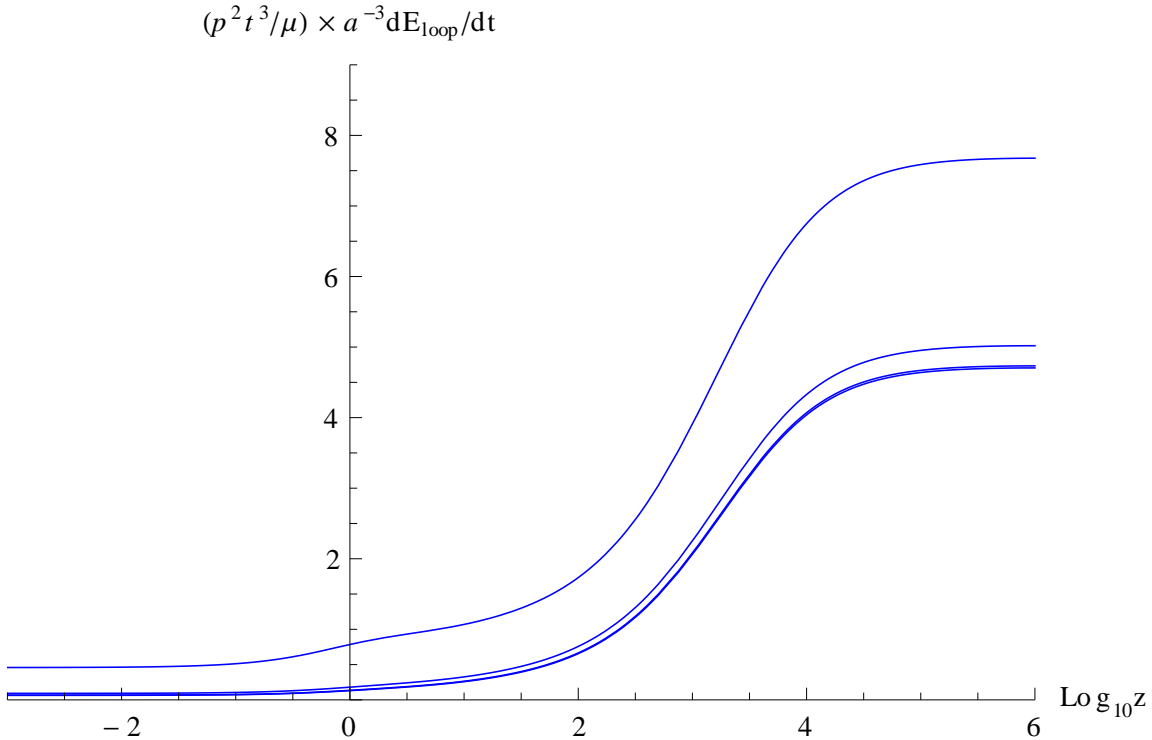


Figure 5: The redshift-dependent rate of energy loss to loops experienced by the string network in Λ CDM cosmology for a given intercommutation probability p . This is important input for predicting properties of today's loops. The ordinate is the dimensionless measure of the rate of energy loss to loops, $\mathcal{A} = \dot{E}_l / (\mu a^3 / (p^2 t^3))$. If the scale factor $a(t)$ were a powerlaw in time then \mathcal{A} would be constant with respect to z . This is not the case in the Λ CDM cosmology with transitions from radiation-to-matter-to- Λ dominated regimes. Different lines show results for $p = 1$ (top) to $p = 10^{-3}$ (bottom) in powers of 10. If network density varied as $1/p^2$ then all these lines would overlap. This is approximately true for small p but not for $p \geq 0.1$.

we have

$$\frac{dn}{dl}(l, t) = \left(\frac{f \mathcal{A} \alpha^2}{p^2} \right) \left(\frac{a(t_b)}{a} \right)^3 \frac{\Phi^3}{(l + \Gamma G \mu t)^4} \quad (7.3)$$

$$t_b = \frac{l + \Gamma G \mu t}{\alpha \Phi} \quad (7.4)$$

$$\Phi = 1 + \frac{\Gamma G \mu}{\alpha}. \quad (7.5)$$

The scaling $dn/dl \propto (l + \Gamma G \mu t)^{-4}$ was already noted by Kibble [136].

The loop number distribution peaks at zero length but the quantity of interest in lensing is number weighted by loop length, $l dn/dl$. The characteristic scale at time t is $l_g = \Gamma G \mu t$, i.e. roughly the size of a newly born loop that would evaporate in total time t . The distribution $l dn/dl$ peaks at $l = (2/3)l_g$.

For $G\mu < 7 \times 10^{-9}(\alpha/0.1)(50/\Gamma)$ the loops near l_g today were born before equipartition, t_{eq} . We use $a \propto t^{1/2}$ to simplify the expression to give

$$l \frac{dn}{dl} = \frac{x}{(1+x)^{5/2}} \left(\frac{f\mathcal{A}}{p^2 t_0^3} \right) (\Gamma G\mu)^{-3/2} \left(\frac{\alpha t_{eq}}{t_0} \right)^{1/2} \quad (7.6)$$

where t_0 is today and $x \equiv l/l_g$.

The numerical results are $\mathcal{A} \sim 7.68$ for $p = 1$, $f = 0.2$, $\alpha = 0.1$ and $\Gamma = 50$ (and from Λ CDM $t_{eq} = 4.7 \times 10^4$ yr and $t_0 = 4.25 \times 10^{17}$ s). These give

$$l \left(\frac{dn}{dl} \right)_{baseline} = 1.15 \times 10^{-6} \frac{x}{(1+x)^{5/2}} \mu_{-13}^{-3/2} \text{ kpc}^{-3} \quad (7.7)$$

$$l_g = 0.0206 \mu_{-13} \text{ pc} \quad (7.8)$$

$$M_g = 0.043 \mu_{-13}^2 M_\odot. \quad (7.9)$$

Here, $\mu_{-13} \equiv G\mu/c^2/10^{-13}$ is an abbreviation for the dimensionless string tension in units of 10^{-13} . The baseline distribution lies below [138, 139] on account of loss of a significant fraction of the network invariant length to small strings and of adoption the Λ CDM cosmology.

Next, string theory modifications to the baseline are lumped into a common factor \mathcal{G}

$$\left(\frac{dn}{dl} \right)_{homog} = \mathcal{G} \left(\frac{dn}{dl} \right)_{baseline} \quad (7.10)$$

to give the description of the actual homogeneous loop distribution. Prominent among expected modifications is the intercommutation factor p . Large scale string simulations have not reached a full understanding of the impact of $p < 1$ though there is no question that \mathcal{G} increases as a result. The numerical treatment of the Velocity One Scale model implies that \mathcal{A} is a weak function of p for small p and, in that limit, $dn/dl \propto 1/p^2$. Ultimately, this matter will be fully settled via network simulations with $p < 1$. String theory calculations of the intercommutation probability suggests $p = 10^{-1}-10^{-3}$ implying $\mathcal{G} = 10^2-10^6$.

The number of populated, non-interacting throats that contain other types of superstrings is a known unknown and is unexplored. In our opinion, there could easily be 100's of such throats for the complicated bulk spaces of interest.

In the string theory scenarios $\mathcal{G} = 1$ is a lower limit. *For the purposes of numerical estimates in this paper we adopt $\mathcal{G} = 10^2$ (with a given tension) as the most reasonable lower limit.* Much larger \mathcal{G} are not improbable while lower \mathcal{G} are unlikely. We should emphasize that strings in different throats would have different tensions, so adopting a single tension here yields only a crude estimate.

7.2 Local string distribution

If a loop is formed at time t with length $l = \alpha t$ then its evaporation time $\tau = l/\Gamma G\mu$. For Hubble constant H at t the dimensionless combination $H\tau = \alpha/(\Gamma G\mu)$ is a

measure of lifetime in terms of the universe’s age. Superstring loops with $\alpha = 0.1$ and small μ live many characteristic Hubble times.

New loops are born with relativistic velocity. The peculiar center of mass motion is damped by the universe’s expansion. A detailed study of the competing effects (formation time, damping, evaporation, efficacy of anisotropic emission of gravitational radiation) in the context of a simple formation model for the galaxy shows that loops accrete when μ is small. The degree of loop clustering relative to dark matter clustering is a function of μ and approximately independent of l . Smaller μ means older, more slowly moving loops and hence more clustering. Below we give a simple fit to the numerical simulations to quantify this effect.

The spatially dependent dark matter enhancement in the galaxy is

$$\mathcal{E}(\vec{r}) = \frac{\rho_{DM}(\vec{r})}{\Omega_{DM}\rho_c} \quad (7.11)$$

where $\rho_{DM}(\vec{r})$ is the local galactic dark matter density and $\Omega_{DM}\rho_c$ is average dark matter density in the universe. Low tension string loops track the dark matter with a certain efficiency as the dark matter forms gravitationally bound structures [133]. We fit the numerical results by writing the spatially dependent string enhancement to the homogeneous distribution as equal to the dark matter enhancement times an efficiency factor

$$\mathcal{F}(\vec{r}) = \mathcal{E}(\vec{r}) 10^{f(y)} \quad (7.12)$$

$$f(y) = \begin{cases} -0.337 - 0.064y^2 - 5(1 + \tanh(y - 7)) & \text{for } 0 \leq y \\ -0.337 & \text{for } y < 0 \end{cases} \quad (7.13)$$

$$y = 2 + \log_{10} \mu_{-13} \quad (7.14)$$

and μ_{-13} is the dimensionless tension in units of 10^{-13} . The clustering is never 100% effective because the string loops eventually evaporate. The efficiency saturates at $y = 0$ or $G\mu/c^2 = 10^{-15}$. The local string population is enhanced by the factor \mathcal{F} with respect to the homogeneous distribution

$$\left(\frac{dn}{dl}\right)_{local}(\vec{r}) = \mathcal{F}(\vec{r}) \left(\frac{dn}{dl}\right)_{homog} = \mathcal{F}(\vec{r}) \mathcal{G} \left(\frac{dn}{dl}\right)_{baseline}. \quad (7.15)$$

To complete the description of the local loop population we adopt empirical fits to the galaxy’s dark matter halo [140]. Model I is a “cored galaxy” center in which the central, limiting dark matter density is zero. Since winds from stars and ejection/heating by supernovae lift baryons out of star-forming regions, the center, they reduce the gravitational potential and tend to lower the dark matter density. Model II is a “cusped galaxy” center in which the density formally diverges. Many N-body simulations show that collisionless structure formation in Λ CDM yields such profiles. The two models are thought to bracket the range of physical possibilities in the central regions and are in general agreement on large scales.

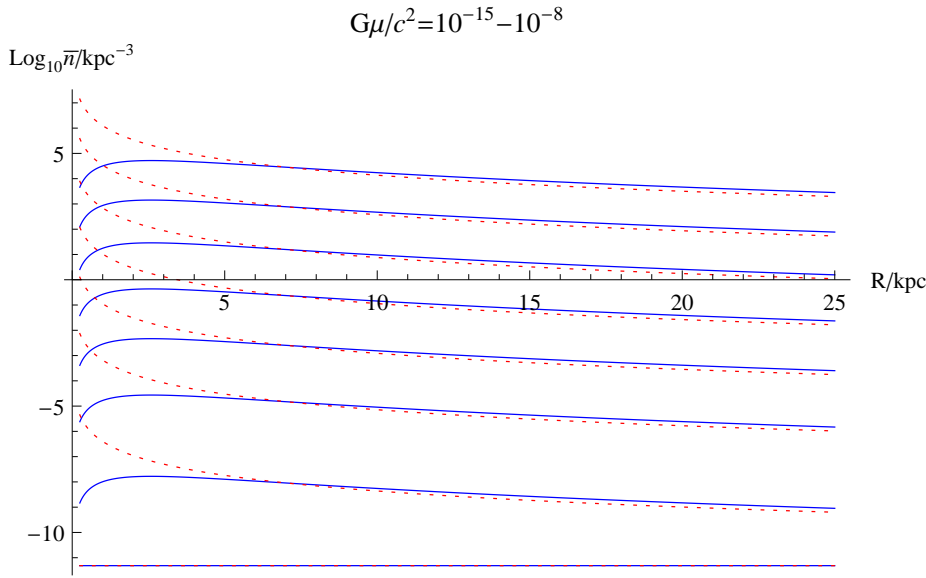


Figure 6: The effective number density of string loops in two galactic models for a range of string tensions. The dotted red lines show results for a galactic model with a cusp at the center, the solid blue lines for a model with a core. The tension is $G\mu/c^2 = 10^{-15}$ for the uppermost curve and increases by powers of 10 until reaching 10^{-8} for the lowest curve. The effective number density depends upon the clustering of loops, the dark matter distribution within the galaxy, the network scaling and loop distribution and \mathcal{G} the enhancement of string theory strings compared to field theory strings.

Let us define the effective number density of loops as the energy density in the distribution of loops of all size, ρ_{loop} , divided by energy of a loop of size equal to the characteristic gravitational cutoff

$$\bar{n} = \frac{\rho_{loop}}{\mu l_g} \quad (7.16)$$

$$= \int dl \frac{dn}{dl} \frac{l}{l_g}. \quad (7.17)$$

Figure 6 plots the effective number density of string loops for two descriptions of the galaxy's dark matter distribution (core and cusp) as a function of galactocentric radius. The different lines show a range of string tensions, all for $\mathcal{G} = 10^2$. The quantity \bar{n} depends upon the efficacy of loop clustering, the dark matter distribution within our galaxy and the network scaling model. There are two curves plotted for each tension. These agree at large radii but differ near the galactic center where the detailed form of the dark matter distribution is uncertain.

For many experiments the rate of detection scales as \bar{n} weighted by powers of l_g . The microlensing rate, for example, is proportional to the product of two factors: the number of string loops along a given line of sight $\propto \bar{n}$ and the length of an individual string loop $\propto l_g$. The event rate scales like $\bar{n} l_g \propto \bar{n} G\mu$. At the Sun's position, the

effective number density increase by ~ 15 orders of magnitude as $G\mu/c^2$ drops from 10^{-8} to 10^{-15} . The microlensing event rate increases by ~ 8 orders of magnitude. As we will discuss shortly, for the same variation in tension the timescale for an individual microlensing event decreases by ~ 8 orders of magnitude. This creates a huge range of timescales of interest for the duration and rate of microlensing events.

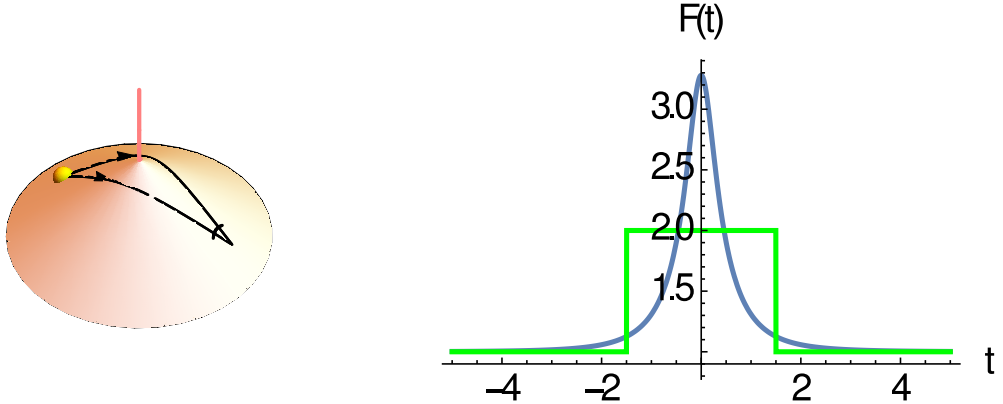


Figure 7: (Left) The conical space-time geometry near a short segment of string (red line) permits photons to travel two paths (black arrows) from source (yellow ball) to observer when source, string and observer are nearly aligned. The ideal observer perceives two images of the source split by a small angle (black arc) proportional in size to string tension. For low string tension, the observer cannot resolve the separate images; however, the flux may be easily measured to be twice that of a single image (in the point source limit) at each wavelength (negligible Kaiser-Stebbins effect). (Right) The microlensing amplification of flux for a point source as a function of time for a string (green) is compared to a Newtonian point masses (blue; the ratio of impact parameter to Einstein radius is 0.31). No other known astrophysical sources produce this *digital* microlensing.

8. Detection

8.1 Detection via Microlensing

Consider a straight segment of string oriented perpendicular to the observer's line of sight with respect to a background source as shown in Figure 7. Let two photons from the source travel towards the string. The photons do not suffer any relative deflection during the fly-by as long as they pass around the string in the same sense. However, there is a small angular region about the string with two paths from the source to the observer. Background sources within angle $\Theta_E = 8\pi G\mu = 1.04 \times 10^{-3}(G\mu/2 \times 10^{-10})$ arcsec form two images. Unlike the case of a point mass, shear and distortion are absent. The angular size of a sun-like star at distance R is $\Theta_\odot/\Theta_E = 4.5 \times 10^{-4}(2 \times 10^{-10}/G\mu)(10\text{kpc}/R)$ so galactic stellar sources generally appear point-like for $G\mu \gtrsim 10^{-13}$.

Compact halo objects lens background sources [141, 142] and unresolved, lensed sources will appear to fluctuate achronatically in brightness. This is microlensing. Experimental efforts to detect microlensing phenomena have borne considerable fruit [143].

Likewise, loops of superstring microlens background sources but have a special

property: the source brightness varies by a factor of 2 as the angular region associated with the string passes across the observer-source line of sight. The amplitude variation, schematically compared in figure 7, is quite distinctive for point sources. The internal motions of a loop are relativistic and generally dominate the motion of the source and the observer. Numerical calculations have established that microlensing occurs when light passes near a relativistic, oscillating string loop [144]; the effect is not limited to a stationary string.

The total rate of lensing R_L implied for a distribution of loops dn/dl is proportional to the solid angle swept out per time $cl/\sqrt{3}r^2$ for loop l at distance r , or $R_L = \int dl dr r^2 dn/dl (cl/\sqrt{3}r^2)$. Small tensions give large lensing rates, $R_L \propto 1/\sqrt{G\mu}$ because the integral over $dn/dl \propto l^{-2.5}$ is dominated by $l \sim l_g$, the gravitational cutoff.

Figure 8 illustrates the hierarchy of relevant timescales. The characteristic duration of the event is $\delta t = R\Theta_E/c \sim 630 \text{ s } (R/10 \text{ kpc })(G\mu/2 \times 10^{-10})$. Loops bound to the galaxy have center-of-mass motions $v_h \sim 220 \text{ km s}^{-1}$; microlensing of a given source will repeat $\sim c/v_h$ times; *new* sources are lensed at rate $\sim (v_h/c)R_L$. The characteristic loop oscillation timescale which governs the intervals in repetitive microlensing of a single source is $t_{osc} \sim l_g/c = 135 \text{ yr } (G\mu/2 \times 10^{-10})$.

The unique fingerprint of loop lensing is *repeated achromatic flux doubling* (digital microlensing). Detection efficiency for digital lensing depends upon the string tension, the magnitude and angular size of the background stars and the time sampling of the observations. Estimates can be made for any experiment which repeatedly measures the flux of stellar sources.

The first string microlensing search [145] was recently completed using photometric data from space-based missions CoRoT²[146] and RXTE³[147]. The methodology was potentially capable of detecting strings with tensions $10^{-16} < G\mu < 10^{-11}$ though the expected number of detections was limited by the available lines of sight studied in the course of the missions. In principle, any photometry experiment that makes repeated flux measurements of an intrinsically stable astronomical source has the power to limit a combination of the number density of loops and string tension. One interesting possibility is the satellite GAIA launched by the European Space Agency in December 2013 designed for astrometry. It is monitoring each of about 1 billion stars about 70 times over a period of 5 years. Another is the Large Synoptic Survey Telescope (LSST) to be sited in Chile within the decade to photograph the entire observable sky every few days. Previous estimates for the rate of detections for GAIA [132] and LSST [148] were encouraging. Now, detailed calculations for WFIRST are also available.

²The 2006 mission was developed and operated by the CNES, with the contribution of Austria, Belgium, Brazil, ESA (RSSD and Science Program), Germany, and Spain.

³The 1995 mission was developed and operated by NASA.

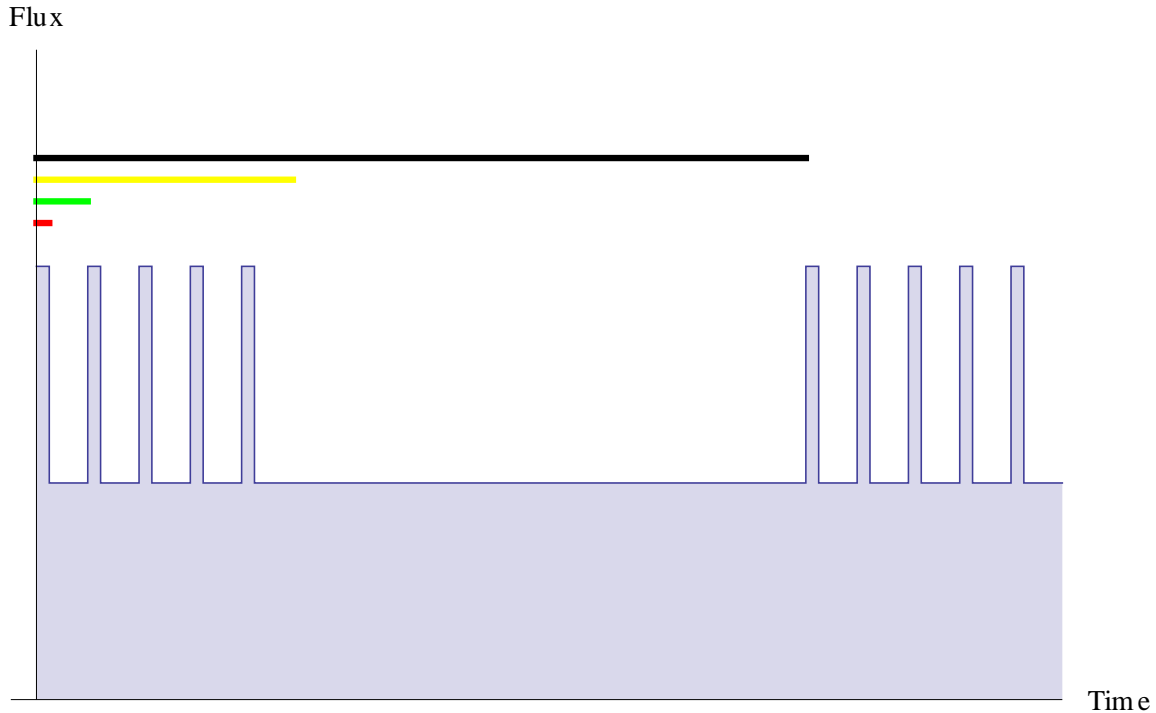


Figure 8: A Schematic Pattern. Digital microlensing doubles the flux over the time period that source, loop and observer are aligned within the deficit angle created by the string (red line). The repetition interval for lensing a particular source is the loop oscillation timescale (green line) and $\sim 10^3$ repetitions in total occur (yellow line). The timescale for a new source to be lensed by the original loop (or the original source by a new loop) is much longer (black line).

8.2 WFIRST Microlensing Rates

The Wide-Field Infrared Survey Telescope⁴ (WFIRST) is a NASA space observatory designed to perform wide-field imaging and slitless spectroscopic surveys of the near infrared sky. WFIRST will carry out a microlensing survey program for exo-planet detection in the direction of the galactic bulge by observing a total of 2.8 square degrees for 1.2 years primarily in a broad long wavelength filter (W-band $0.927 - 2.0\mu\text{m}$). Repeated, short exposures (~ 1 minute) of the same fields are the key to searching for and to monitoring the amplification of bulge sources by star-planet systems along the line of sight. Fortuitously, the WFIRST experiment is also sensitive to cosmic strings.

We have evaluated⁵ the expected microlensing rate by cosmic strings for a realistic distribution of stars (stellar types, distances, velocities, etc.), dust obscuration and survey parameters (flux sensitivity, time of exposure and angular scale of stars). The lensing rate is split into digital events (the flux doubles), analog events (all po-

⁴<http://wfirst.gsfc.nasa.gov/>

⁵Material in this section[149]

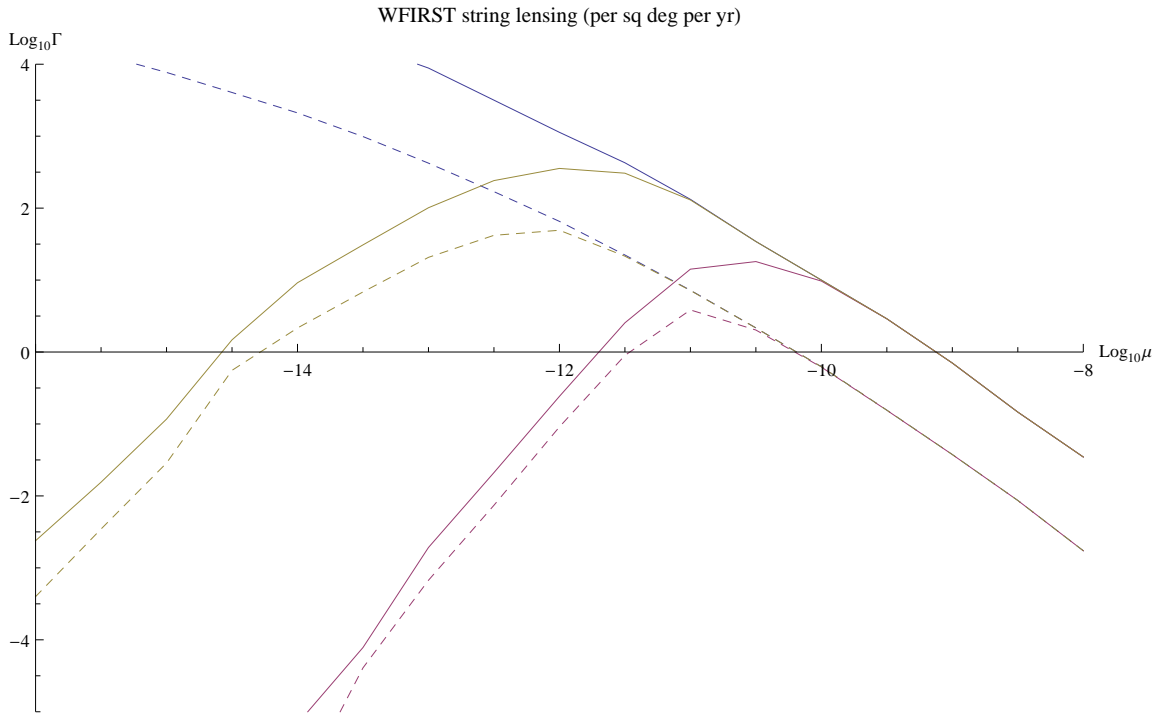


Figure 9: The intrinsic string lensing rate (events per sq degree per year) for WFIRST’s study of the bulge for $\mathcal{G} = 10^2$. The three solid lines show digital (red), analog (green) and total (blue) event rates for the dark matter model with a cusp. The three dashed lines (same meaning for the colors) give the event rate for the model with a core. The analog rate does not account for blending which may diminish the detectable rate by no more than a factor of 10.

tentially measurable flux enhancements given the signal-to-noise of the observations) and total events (all geometric configurations that can lens, whether detectable or not) evaluated for two galactic dark matter models (with cusp and with core at galactic center). Figure 9 shows the string lensing rate per square degree as a function of string tension $G\mu/c^2$ for $\mathcal{G} = 10^2$. The lensing rate for digital and analog events exceeds 10 per square degree per year for $10^{-14} < G\mu/c^2 < 10^{-10}$ for the cusp model and for $10^{-13} < G\mu/c^2 < 10^{-11}$ for the core model. The results for the cusp and core models should be regarded as establishing the range of astrophysical possibilities for the loop density distribution within the experiment. The range of string theory possibilities (the variation of \mathcal{G}) remains substantial. Digital and *spatially resolved* analog events can be reliably detected. Blending of sources in analog events needs to be simulated to fully characterize the fraction of such events that will be detectable. In any case, the decrease from blending is limited: sources brighter than magnitude 23 in the J-band ($1.131 - 1.454\mu\text{m}$) contribute at least 10% of the total analog rate, are well-separated and produce light curves detectable at high signal-to-noise.

These results show that WFIRST microlensing searches can probe hitherto un-

explored ranges of string tension. Future surveys of wider areas of the bulge and/or surveys lasting for longer periods of time can potentially scale up the total expected rate of detection by as much as 100. Surveys with shorter exposures times are able to discern larger numbers of digital events.

8.3 Gravitational Waves

Besides uncovering a relic from the earliest moments of the universe’s formation, the observation of a superstring microlensing event provides some immediate information. If the event is resolved in time, the characteristic *string tension* is inferred. If repetitions are seen, the characteristic *loop size* is constrained. And any detection provides a precise sky location for follow up. Some classes of strings create electromagnetic signatures but all generate gravitational radiation possibly observable by LISA-like (hereafter, LISA) and LIGO-like instruments.

The scenario that LISA detects the distinctive signature of local loop emission has been contemplated for a blind, all-sky search [150]. They relied on the enhancement from local clustering [132] and concluded that strings with $10^{-19} < G\mu < 10^{-11}$ were potentially detectable via fundamental and low-order harmonics. They also estimated the background from the galaxy and from the universe as a whole.

Therefore, it is no surprise that a loop microlensing event offers some exciting possibilities. The key considerations are: (1) The precise location afforded by microlensing dramatically reduces the signal search space on the sky. (2) A generic loop radiates a full range of harmonics with frequency $f_n = nf_1 = 2cn/l$ because the equations of motion are intrinsically non-linear. (3) Many string harmonics fall near LISA’s peak sensitivity $n_* = f_*/f_1 \gg 1$ ($h_{LISA} \sim 10^{-23.8}$ at $f_* \sim 10^{-2.3}$ Hz for 1 year periodic variation [151]; tension $\mu_{crit} = 2.9 \times 10^{-12}$ corresponds to a 1 year period; $n_* = 1.6 \times 10^5(\mu/\mu_{crit})$). (4) Galactic binary interference becomes problematic only at $f < f_{WD}$ where $f_{WD} \sim 10^{-2.6}$ Hz [152].

LISA’s verification binaries have known positions on the sky, orbital frequencies, masses, distance limits etc. determined by optical measurements and other means [151]. A long-lived superstring loop detected by microlensing shares similar observational advantages: it has known position on the sky, distance upper limit estimated based on the microlensed star and emits a distinctive signal. This creates the ideal observational situation in which much of the data analysis can be conducted with a single fast Fourier transform.

Different types of loops generate different gravitational wave signatures. The solution for a Nambu-Goto loop’s motion is the sum of left and right-moving one-dimensional waves subject to nonlinear constraints. When both modes are smooth (no derivative discontinuities) the dynamical solution can form a cusp. At that instant a bit of the string reaches the speed of light. When one mode is smooth but the other has a discontinuity the loop’s dynamical solution includes a kink, a discontinuity in the string’s tangent vector that moves along the string at the speed

of light in one direction. When both modes have discontinuities we call the solution a k-kink. The presence of cusps, kinks and k-kinks may be inferred from the paths of the tangent vectors of the left and right moving modes which are constrained to lie on the surface of a sphere.

These distinctions are relevant for gravitational wave emission: the cusp generates bursts of beamed radiation, the kink has a pulsar-like beam that generically sweeps across a substantial angle in the sky and the k-kink emits into a substantial fraction of the sky. We model the beaming anisotropy, the harmonic power and phase of the gravitational wave signal (qualitatively and quantitatively extending previous analyses [150]). Standard signal detection theory characterizes the strength of detection and the precision with which measurements can be made by comparing the putative signal to noise sources. Here, we consider only detector noise described as an additive, stationary, random Gaussian process with one-sided spectral noise at frequency f is $S(\|f\|)$. The strength of signal $h(t)$ is $\rho_{SNR} = \sqrt{2 \langle h, h \rangle}$ where the symmetric inner product is $\langle g, h \rangle = \int_{-\infty}^{\infty} df \frac{\tilde{g}(f)\tilde{h}^*(f)}{S(\|f\|)}$ and $\tilde{g}(f)$ is the Fourier transform of $g(t)$ (the factor of 2 stems from one-sided noise versus two-sided signal). Figure 10 summarizes ρ_{SNR} for detecting a single source with beamed cusp, beamed kink and generic, unbeamed emission. Upper and lower line pairs show the effect of ignoring and accounting for the galactic white dwarf interference. Confusion is minimal because the string signal extends to frequencies where the binary density is small and because the signal overlap between string and binary sources is small.

The time-averaged microlensing rate is roughly proportional to the loop's maximum projected area divided by its period of oscillation but the gravitational wave emissivity is dominated by specific loop configurations having rapidly moving segments when the loop is most contracted. Microlensing and beamed, gravitational wave emission generally will not and need not be simultaneous to be informative. We elaborate on this important point.

Generic cusps and kinks have characteristic beaming patterns described above and undergo fully three dimensional motions that yield time-averaged microlensing rates that are not particularly angle-dependent. Microlensing is a favorable means to locate such loops but the high frequency, directed gravitational wave beams they emit are visible only from special directions. A microlensing detection does not significantly influence the probability of intercepting beamed emission in experiments with duration exceeding the fundamental loop period. Instead, there is a roughly constant, low probability that a cusp that is present will beam in the observer's direction and modest probability that a kink will (the beam's angular size is smaller at higher frequencies of emission).

The most likely configuration for k-kinks is a flat, degenerate box-like orbit with a well-defined plane. Special observers who lie in that plane will not see microlensing but most others are sensitive to the loop's projected motion and see the effect if a

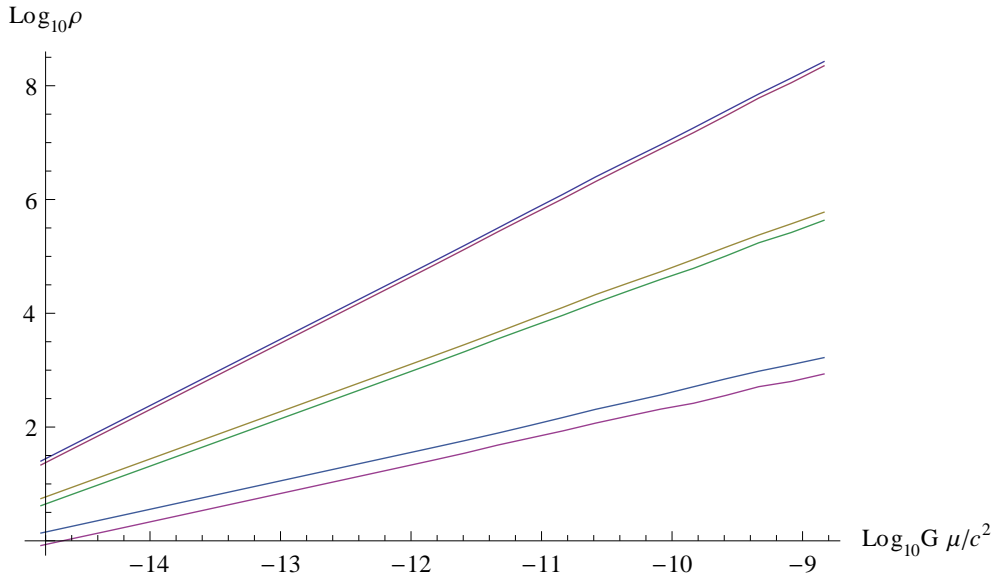


Figure 10: The log of LISA’s signal strength ($\log_{10} \rho_{SNR}$) for 1 year of observation of cusp, kink and k-kink (top to bottom) at a distance of 1 kpc with a known position on the sky as a function of string tension. The orientation of the cusp and kink is for the maximum signal. Upper/lower line pairs show the effect of ignoring/accounting for white dwarf interference. For tensions with $G\mu/c^2 > 3 \times 10^{-12}$ the fundamental loop period exceeds the length of the observation so excess power is seen but the frequency resolution is insufficient to measure individual harmonics.

suitable background source exists. The gravitational wave emission of galactic k-kinks is not strongly beamed but, as the signal estimates show, is still potentially detectable. Unbeamed emission from loops that happen to contain cusps and kinks should also be detectable whether or not the high frequency beam impinges on the observer.

To summarize, there are excellent chances to detect some of this emission once the precise location of the source is known. If the fundamental string period is less than the duration of the experiment then the string’s frequency comb can be resolved and fit. Otherwise, there will be excess frequency-dependent power seen in the microlensing direction. The issue of confusion with local and cosmological string loops will be addressed in future studies.

While non-detection by LISA would place bounds on tension and loop size the most informative scenario will be measuring the individual harmonics of gravitational wave emission. Cusps have almost smooth spectral amplitude and phase distributions, kinks show some mode-to-mode variation and k-kinks progressively more. The variation with harmonic order provides immediate information regarding derivative discontinuities, e.g. *an experimental determination of cusp and kink content*. This is directly applicable for understanding the string network in a cosmological context. Specifically, the discontinuities are created when horizon-crossing strings are chopped

into loops but are modified as the strings are stretched out by the expanding universe. It is important to understand if the loops exclusively contain discontinuities or, also, cusps. This relates to anticipated cosmologically distant string sources that contribute to the gravitational wave background currently sought.

A measurement of the fundamental frequency is equivalent to a precise measurement of the invariant string length. It can be determined in 1 year to relative accuracy at least as good as $\Delta f_1/f_1 \sim 1/\rho_{SNR}$. The gravitational decay time for the typical string loop is likely to be of order the age of universe. A study of Figure 10 suggests that the expected decay in a year $\Delta f_1/f_1 \sim 10^{-10}$ is too small to measure directly unless the loop is unexpectedly close to the end of its life or very nearby. Instead, first, one will measure changes in frequency from center of mass motion and acceleration within the galaxy and place upper limits on $\Delta f_1/f_1$. The latter will constrain string couplings to axion-like fields and astrophysical effects of nearby matter. Since loops are long-lived sources emitting over a wide range of harmonics, eventually, multiple detectors will be brought to bear and the loop's decay measured in a direct fashion. This program can yield a precise determination of the string tension.

We thank Jolyon Bloomfield, Tom Broadhurst, Jim Cordes, John Ellis, Eanna Flanagan, Romain Graziani, Mark Hindmarsh, Renata Kallosh, Andrei Linde, Liam McAllister, Levon Pogosian, Ben Shlaer, Yoske Sumitomo, Alex Vilenkin, Barry Wardell, Ira Wasserman and Sam Wong for discussions. We gratefully acknowledge the support of the John Templeton Foundation (Univ. of Chicago 37426-Cornell FP050136-B). SHHT is supported by the CRF Grants of the Government of the Hong Kong SAR under HUKST4/CRF/13G.

References

- [1] A. H. Guth, *Inflationary universe: A possible solution to the horizon and flatness problems*, *Physical Review D* **23** (Jan., 1981) 347–356.
- [2] A. D. Linde, *A new inflationary universe scenario: a possible solution of the horizon, flatness, homogeneity, isotropy and primordial monopole problems.*, *Physics Letters B* **108** (1982) 389–393.
- [3] A. Albrecht and P. J. Steinhardt, *Cosmology for grand unified theories with radiatively induced symmetry breaking*, *Physical Review Letters* **48** (Apr., 1982) 1220–1223.
- [4] D. Baumann and L. McAllister, *Inflation and String Theory*, *ArXiv e-prints* *1404.2601* (2014).
- [5] A. Vilenkin and E. P. S. Shellard, *Cosmic Strings and Other Topological Defects*. July, 2000.

- [6] P. Ade *et al.*, *Detection of B-Mode Polarization at Degree Angular Scales by BICEP2*, *Phys.Rev.Lett.* **112** (2014) 241101.
- [7] R. Flauger, J. C. Hill, and D. N. Spergel, *Toward an Understanding of Foreground Emission in the BICEP2 Region*, *ArXiv e-prints 1405.7351* (May, 2014).
- [8] M. J. Mortonson and U. Seljak, *A joint analysis of Planck and BICEP2 B modes including dust polarization uncertainty*, *ArXiv e-prints 1405.5857* (May, 2014).
- [9] G. F. Smoot, C. L. Bennett, A. Kogut, E. L. Wright, J. Aymon, N. W. Boggess, E. S. Cheng, G. de Amici, S. Gulkis, M. G. Hauser, G. Hinshaw, P. D. Jackson, M. Janssen, E. Kaita, T. Kelsall, P. Keegstra, C. Lineweaver, K. Loewenstein, P. Lubin, J. Mather, S. S. Meyer, S. H. Moseley, T. Murdock, L. Rokke, R. F. Silverberg, L. Tenorio, R. Weiss, and D. T. Wilkinson, *Structure in the COBE differential microwave radiometer first-year maps*, *Astrophysical Journal* **396** (Sept., 1992) L1–L5.
- [10] Planck Collaboration, P. A. R. Ade, N. Aghanim, C. Armitage-Caplan, M. Arnaud, M. Ashdown, F. Atrio-Barandela, J. Aumont, C. Baccigalupi, A. J. Banday, and *et al.*, *Planck 2013 results. XXII. Constraints on inflation*, *ArXiv e-prints 1303.5082* (Mar., 2013).
- [11] D. H. Lyth, *What would we learn by detecting a gravitational wave signal in the cosmic microwave background anisotropy?*, *Phys.Rev.Lett.* **78** (1997) 1861–1863.
- [12] I. Antoniadis and S. P. Patil, *The Effective Planck Mass and the Scale of Inflation*, *ArXiv e-prints 1410.8845* (Oct., 2014).
- [13] S. B. Giddings, S. Kachru, and J. Polchinski, *Hierarchies from fluxes in string compactifications*, *Phys.Rev.* **D66** (2002) 106006.
- [14] S. Kachru, R. Kallosh, A. D. Linde, and S. P. Trivedi, *De Sitter vacua in string theory*, *Phys.Rev.* **D68** (2003) 046005.
- [15] M. R. Douglas and S. Kachru, *Flux compactification*, *Rev.Mod.Phys.* **79** (2007) 733–796.
- [16] R. Bousso and J. Polchinski, *Quantization of four form fluxes and dynamical neutralization of the cosmological constant*, *JHEP* **0006** (2000) 006.
- [17] Y. Sumitomo and S.-H. H. Tye, *A stringy mechanism for a small cosmological constant — multi-moduli cases*, *Journal of Cosmology and Astroparticle Physics* **2** (Feb., 2013) 6.
- [18] K. Freese, J. A. Frieman, and A. V. Olinto, *Natural inflation with pseudo Nambu-Goldstone bosons*, *Physical Review Letters* **65** (Dec., 1990) 3233–3236.

- [19] F. C. Adams, J. R. Bond, K. Freese, J. A. Frieman, and A. V. Olinto, *Natural inflation: Particle physics models, power-law spectra for large-scale structure, and constraints from the Cosmic Background Explorer*, *Physical Review D* **47** (Jan., 1993) 426–455.
- [20] G. Dvali and S. H. Tye, *Brane inflation.*, *Physics Letters B* **450** (Mar., 1999) 72–82.
- [21] C. P. Burgess, M. Majumdar, D. Nolte, F. Quevedo, G. Rajesh, and R.-J. Zhang, *The inflationary brane-antibrane universe*, *Journal of High Energy Physics* **7** (July, 2001) 47.
- [22] G. Dvali, Q. Shafi, and S. Solganik, *D-brane inflation*, *ArXiv e-prints hep/th/0105203* (May, 2001).
- [23] S. Kachru, R. Kallosh, A. D. Linde, J. M. Maldacena, L. P. McAllister, *et al.*, *Towards inflation in string theory*, *JCAP* **0310** (2003) 013.
- [24] C. Burgess, R. Kallosh, and F. Quevedo, *De Sitter string vacua from supersymmetric D terms*, *JHEP* **0310** (2003) 056.
- [25] M. Berg, M. Haack, and B. Kors, *On the moduli dependence of nonperturbative superpotentials in brane inflation*, *ArXiv e-prints hep-th/0409282* (2004).
- [26] D. Baumann, A. Dymarsky, I. R. Klebanov, J. M. Maldacena, L. P. McAllister, *et al.*, *On D3-brane Potentials in Compactifications with Fluxes and Wrapped D-branes*, *JHEP* **0611** (2006) 031.
- [27] S. Buchan, B. Shlaer, H. Stoica, and S. H. Tye, *Inter-brane interactions in compact spaces and brane inflation*, *Journal of Cosmology and Astro-Particle Physics* **02** (Feb., 2004) 013.
- [28] H. Firouzjahi and S.-H. H. Tye, *Brane inflation and cosmic string tension in superstring theory*, *JCAP* **0503** (2005) 009.
- [29] R. Bean, X. Chen, G. Hailu, S.-H. H. Tye, and J. Xu, *Duality Cascade in Brane Inflation*, *JCAP* **0803** (2008) 026.
- [30] A. Krause and E. Pajer, *Chasing brane inflation in string theory*, *Journal of Cosmology and Astroparticle Physics* **7** (July, 2008) 23.
- [31] E. Silverstein and D. Tong, *Scalar speed limits and cosmology: Acceleration from D-celeration*, *Physical Review D* **70** (Nov., 2004) 103505.
- [32] M. Alishahiha, E. Silverstein, and D. Tong, *DBI in the sky: Non-Gaussianity from inflation with a speed limit*, *Physical Review D* **70** (Dec., 2004) 123505.
- [33] X. Chen, *Multithroat brane inflation*, *Physical Review D* **71** (Mar., 2005) 063506.
- [34] X. Chen, *Inflation from warped space*, *Journal of High Energy Physics* **8** (Aug., 2005) 45.

- [35] K. Dasgupta, C. Herdeiro, S. Hirano, and R. Kallosh, *D3-D7 inflationary model and M theory*, *Physical Review D* **65** (June, 2002) 126002.
- [36] J. P. Conlon and F. Quevedo, *Kähler moduli inflation*, *Journal of High Energy Physics* **1** (Jan., 2006) 146.
- [37] J. E. Kim, H. P. Nilles, and M. Peloso, *Completing natural inflation*, *JCAP* **0501** (2005) 005.
- [38] E. Silverstein and A. Westphal, *Monodromy in the CMB: Gravity waves and string inflation*, *Physical Review D* **78** (Nov., 2008) 106003.
- [39] L. McAllister, E. Silverstein, and A. Westphal, *Gravity Waves and Linear Inflation from Axion Monodromy*, *Phys.Rev.* **D82** (2010) 046003.
- [40] A. D. Linde, *Chaotic Inflation*, *Phys.Lett.* **B129** (1983) 177–181.
- [41] K. Freese and W. H. Kinney, *Natural Inflation: Consistency with Cosmic Microwave Background Observations of Planck and BICEP2*, *ArXiv e-prints 1403.5277* (2014).
- [42] S. Dimopoulos, S. Kachru, J. McGreevy, and J. G. Wacker, *N-flation*, *Journal of Cosmology and Astroparticle Physics* **8** (Aug., 2008) 3.
- [43] R. Easther and L. McAllister, *Random matrices and the spectrum of N-flation*, *Journal of Cosmology and Astroparticle Physics* **5** (May, 2006) 18.
- [44] K. Choi, H. Kim, and S. Yun, *Natural inflation with multiple sub-Planckian axions*, *Phys.Rev.* **90** (July, 2014) 023545.
- [45] S.-H. H. Tye and S. S. C. Wong, *Helical Inflation and Cosmic Strings*, *ArXiv e-prints 1404.6988* (Apr., 2014).
- [46] R. Kappl, S. Krippendorf, and H. P. Nilles, *Aligned Natural Inflation: Monodromies of two Axions*, *ArXiv e-prints 1404.7127* (Apr., 2014).
- [47] I. Ben-Dayan, F. Gil Pedro, and A. Westphal, *Hierarchical Axion Inflation*, *ArXiv e-prints 1404.7773* (Apr., 2014).
- [48] C. Long, L. McAllister, and P. McGuirk, *Aligned natural inflation in string theory*, *Phys.Rev.* **90** (July, 2014) 023501.
- [49] K. Harigaya and M. Ibe, *Inflaton potential on a Riemann surface*, *ArXiv e-prints 1404.3511* (Apr., 2014).
- [50] T. Higaki and F. Takahashi, *Natural and Multi-Natural Inflation in Axion Landscape*, *ArXiv e-prints 1404.6923* (Apr., 2014).
- [51] T. C. Bachlechner, M. Dias, J. Frazer, and L. McAllister, *A New Angle on Chaotic Inflation*, *ArXiv e-prints 1404.7496* (Apr., 2014).

- [52] M. Berg, E. Pajer, and S. Sjors, *Two-field high-scale inflation in a sub-Planckian region of field space*, *Physical Review D* **81** (May, 2010) 103535.
- [53] R. Kallosh, A. Linde, and B. Vercnocke, *Natural Inflation in Supergravity and Beyond*, *ArXiv e-prints 1404.6244* (2014).
- [54] F. Marchesano, G. Shiu, and A. M. Uranga, *F-term Axion Monodromy Inflation*, *ArXiv e-prints 1404.3040* (Apr., 2014).
- [55] L. McAllister, E. Silverstein, A. Westphal, and T. Wrase, *The Powers of Monodromy*, *ArXiv e-prints 1405.3652* (May, 2014).
- [56] M. Arends, A. Hebecker, K. Heimpel, S. C. Kraus, D. Lust, C. Mayrhofer, C. Schick, and T. Weigand, *D7-Brane Moduli Space in Axion Monodromy and Fluxbrane Inflation*, *ArXiv e-prints 1405.0283* (May, 2014).
- [57] M. R. Setare, A. Sepehri, and V. Kamali, *Constructing warm inflationary model in brane-antibrane system*, *Physics Letters B* **735** (July, 2014) 84–89.
- [58] H.-Y. Schive, T. Chiueh, and T. Broadhurst, *Cosmic structure as the quantum interference of a coherent dark wave*, *Nature Physics* **10** (July, 2014) 496–499.
- [59] E. Witten, *Cosmic superstrings.*, *Physics Letters B* **153** (1985) 243–246.
- [60] J. Polchinski, *Dirichlet Branes and Ramond-Ramond Charges*, *Physical Review Letters* **75** (Dec., 1995) 4724–4727.
- [61] L. Randall and R. Sundrum, *Large Mass Hierarchy from a Small Extra Dimension*, *Physical Review Letters* **83** (Oct., 1999) 3370–3373.
- [62] L. Leblond and S.-H. H. Tye, *Stability of D1-Strings Inside a D3-Brane*, *Journal of High Energy Physics* **3** (Mar., 2004) 55.
- [63] E. J. Copeland, R. C. Myers, and J. Polchinski, *Cosmic f- and d-strings*, *Journal of High Energy Physics* **06** (June, 2004) 013.
- [64] H. Firouzjahi, L. Leblond, and S. H. H. Tye, *The (p,q) string tension in a warped deformed conifold*, *Journal of High Energy Physics* **5** (May, 2006) 47.
- [65] A. Avgoustidis, S. Chadburn, and R. Gregory, *Cosmic superstring trajectories in warped compactifications*, *Physical Review D* **86** (Sept., 2012) 063516.
- [66] C. L. Bennett, A. J. Banday, K. M. Gorski, G. Hinshaw, P. Jackson, P. Keegstra, A. Kogut, G. F. Smoot, D. T. Wilkinson, and E. L. Wright, *Four-Year COBE DMR cosmic microwave background observations: Maps and basic results*, *Astrophysical Journal* **464** (June, 1996) L1.
- [67] D. N. Spergel, R. Bean, O. Dor, M. R. Nolta, C. L. Bennett, J. Dunkley, G. Hinshaw, N. Jarosik, E. Komatsu, L. Page, H. V. Peiris, L. Verde, M. Halpern,

- R. S. Hill, A. Kogut, M. Limon, S. S. Meyer, N. Odegard, G. S. Tucker, J. L. Weiland, E. Wollack, and E. L. Wright, *Three-Year wilkinson microwave anisotropy probe (WMAP) observations: Implications for cosmology*, *Astrophysical Journal Supplement Series* **170** (June, 2007) 377–408.
- [68] N. Jones, H. Stoica, and S. H. Tye, *Brane interaction as the origin of inflation*, *Journal of High Energy Physics* **07** (July, 2002) 051.
- [69] S. Sarangi and S. H. Tye, *Cosmic string production towards the end of brane inflation*, *Physics Letters B* **536** (June, 2002) 185–192.
- [70] N. T. Jones, H. Stoica, and S. H. Tye, *The production, spectrum and evolution of cosmic strings in brane inflation*, *Physics Letters B* **563** (June, 2003) 6–14.
- [71] H. Firouzjahi and S. H. Tye, *Brane inflation and cosmic string tension in superstring theory*, *Journal of Cosmology and Astro-Particle Physics* **03** (Mar., 2005) 009.
- [72] S. E. Shandera and S. H. Tye, *Observing brane inflation*, *Journal of Cosmology and Astro-Particle Physics* **05** (May, 2006) 007.
- [73] M. G. Jackson, N. T. Jones, and J. Polchinski, *Collisions of cosmic f- and d-strings*, *Journal of High Energy Physics* **10** (Oct., 2005) 013.
- [74] A. Vilenkin, *Gravitational field of vacuum domain walls*, *Physics Letters B* **133** (Dec., 1983) 177–179.
- [75] C. Hogan and R. Narayan, *Gravitational lensing by cosmic strings*, *Monthly Notices of the Royal Astronomical Society* **211** (Dec., 1984) 575–591.
- [76] A. Vilenkin, *Cosmic strings as gravitational lenses*, *Astrophysical Journal* **282** (July, 1984) L51–L53.
- [77] A. A. de Laix, *Observing long cosmic strings through gravitational lensing*, *Physical Review D* **56** (Nov., 1997) 6193–6204.
- [78] F. Bernardeau and J. Uzan, *Cosmic string lens phenomenology: Model of poisson energy distribution*, *Physical Review D* **63** (Jan., 2001) 23005.
- [79] M. Sazhin, G. Longo, M. Capaccioli, J. M. Alcal, R. Silvotti, G. Covone, O. Khovanskaya, M. Pavlov, M. Pannella, M. Radovich, and V. Testa, *CSL-1: chance projection effect or serendipitous discovery of a gravitational lens induced by a cosmic string?*, *Monthly Notices of the Royal Astronomical Society* **343** (Aug., 2003) 353–359.
- [80] M. V. Sazhin, M. Capaccioli, G. Longo, M. Paolillo, O. S. Khovanskaya, N. A. Grogin, E. J. Schreier, and G. Covone, *The true nature of CSL-1*, *ArXiv e-prints astro-ph/0601494* (Jan., 2006).

- [81] J. L. Christiansen, E. Albin, K. A. James, J. Goldman, D. Maruyama, and G. F. Smoot, *Search for cosmic strings in the Great Observatories Origins Deep Survey*, *Physical Review D* **77** (June, 2008) 123509.
- [82] J. L. Christiansen, E. Albin, T. Fletcher, J. Goldman, I. P. W. Teng, M. Foley, and G. F. Smoot, *Search for cosmic strings in the COSMOS survey*, *Physical Review D* **83** (June, 2011) 122004.
- [83] C. Hogan and R. Narayan, *Gravitational lensing by cosmic strings*, *Monthly Notices of the Royal Astronomical Society* **211** (Dec., 1984) 575–591.
- [84] T. Vachaspati and A. Vilenkin, *Gravitational radiation from cosmic strings*, *Physical Review D* **31** (June, 1985) 3052–3058.
- [85] A. Economou, D. Harari, and M. Sakellariadou, *Gravitational effects of traveling waves along global cosmic strings*, *Physical Review D* **45** (Jan., 1992) 433–440.
- [86] R. A. Battye, R. R. Caldwell, and E. P. S. Shellard, *Gravitational Waves from Cosmic Strings*, in *Topological Defects in Cosmology* (M. Signore and F. Melchiorri, eds.), p. 11, 1998.
- [87] T. Damour and A. Vilenkin, *Gravitational wave bursts from cosmic strings*, *Physical Review Letters* **85** (Oct., 2000) 3761–3764.
- [88] T. Damour and A. Vilenkin, *Gravitational wave bursts from cusps and kinks on cosmic strings*, *Physical Review D* **64** (Sept., 2001) 64008.
- [89] T. Damour and A. Vilenkin, *Gravitational radiation from cosmic (super)strings: Bursts, stochastic background, and observational windows*, *Physical Review D* **71** (Mar., 2005) 63510.
- [90] X. Siemens, J. Creighton, I. Maor, S. R. Majumder, K. Cannon, and J. Read, *Gravitational wave bursts from cosmic (super)strings: Quantitative analysis and constraints*, *Physical Review D* **73** (May, 2006) 105001.
- [91] C. J. Hogan, *Gravitational waves from light cosmic strings: Backgrounds and bursts with large loops*, *Physical Review D* **74** (Aug., 2006) 43526.
- [92] X. Siemens, V. Mandic, and J. Creighton, *Gravitational-Wave stochastic background from cosmic strings*, *Physical Review Letters* **98** (Mar., 2007) 111101.
- [93] B. Abbott et al., *Searches for periodic gravitational waves from unknown isolated sources and scorpius x-1: Results from the second LIGO science run*, *Physical Review D* **76** (Oct., 2007) 82001.
- [94] B. P. Abbott, R. Abbott, R. Adhikari, P. Ajith, B. Allen, G. Allen, R. S. Amin, S. B. Anderson, W. G. Anderson, M. A. Arain, and et al., *First LIGO search for gravitational wave bursts from cosmic (super)strings*, *Physical Review D* **80** (Sept., 2009) 062002.

- [95] B. P. Abbott et al., The LIGO Collaboration, and The Virgo Collaboration, *An upper limit on the stochastic gravitational-wave background of cosmological origin*, *Nature* **460** (Aug., 2009) 990–994.
- [96] J. Aasi, J. Abadie, B. P. Abbott, R. Abbott, T. Abbott, M. R. Abernathy, T. Accadia, F. Acernese, C. Adams, T. Adams, and et al., *Constraints on Cosmic Strings from the LIGO-Virgo Gravitational-Wave Detectors*, *Physical Review Letters* **112** (Apr., 2014) 131101.
- [97] F. R. Bouchet and D. P. Bennett, *Millisecond-pulsar constraint on cosmic strings*, *Physical Review D* **41** (Jan., 1990) 720–723.
- [98] R. R. Caldwell and B. Allen, *Cosmological constraints on cosmic-string gravitational radiation*, *Physical Review D* **45** (May, 1992) 3447–3468.
- [99] V. M. Kaspi, J. H. Taylor, and M. F. Ryba, *High-precision timing of millisecond pulsars. 3: Long-term monitoring of PSRs b1855+09 and b1937+21*, *Astrophysical Journal* **428** (June, 1994) 713–728.
- [100] F. A. Jenet, G. B. Hobbs, W. van Straten, R. N. Manchester, M. Bailes, J. P. W. Verbiest, R. T. Edwards, A. W. Hotan, J. M. Sarkissian, and S. M. Ord, *Upper bounds on the Low-Frequency stochastic gravitational wave background from pulsar timing observations: Current limits and future prospects*, *Astrophysical Journal* **653** (Dec., 2006) 1571–1576.
- [101] M. R. Depies and C. J. Hogan, *Stochastic gravitational wave background from light cosmic strings*, *Physical Review D* **75** (June, 2007) 125006.
- [102] P. B. Demorest, R. D. Ferdman, M. E. Gonzalez, D. Nice, S. Ransom, I. H. Stairs, Z. Arzoumanian, A. Brazier, S. Burke-Spolaor, S. J. Chamberlin, J. M. Cordes, J. Ellis, L. S. Finn, P. Freire, S. Giampanis, F. Jenet, V. M. Kaspi, J. Lazio, A. N. Lommen, M. McLaughlin, N. Palliyaguru, D. Perrodin, R. M. Shannon, X. Siemens, D. Stinebring, J. Swiggum, and W. W. Zhu, *Limits on the Stochastic Gravitational Wave Background from the North American Nanohertz Observatory for Gravitational Waves*, *Astrophysical Journal* **762** (Jan., 2013) 94.
- [103] L. Pogosian, S. H. Tye, I. Wasserman, and M. Wyman, *Observational constraints on cosmic string production during brane inflation*, *Physical Review D* **68** (July, 2003) 23506.
- [104] L. Pogosian, M. Wyman, and I. Wasserman, *Observational constraints on cosmic strings: Bayesian analysis in a three-dimensional parameter space*, *Journal of Cosmology and Astro-Particle Physics* **09** (Sept., 2004) 008.
- [105] S. H. Tye, I. Wasserman, and M. Wyman, *Scaling of multitenion cosmic superstring networks*, *Physical Review D* **71** (May, 2005) 103508.

- [106] M. Wyman, L. Pogosian, and I. Wasserman, *Bounds on cosmic strings from WMAP and SDSS*, *Physical Review D* **72** (July, 2005) 23513.
- [107] L. Pogosian, I. Wasserman, and M. Wyman, *On vector mode contribution to CMB temperature and polarization from local strings*, *ArXiv Astrophysics e-prints* (Apr., 2006).
- [108] U. Seljak, A. Slosar, and P. McDonald, *Cosmological parameters from combining the Lyman-forest with CMB, galaxy clustering and SN constraints*, *Journal of Cosmology and Astro-Particle Physics* **10** (Oct., 2006) 014.
- [109] N. Bevis, M. Hindmarsh, M. Kunz, and J. Urrestilla, *CMB power spectrum contribution from cosmic strings using field-evolution simulations of the abelian Higgs model*, *Physical Review D* **75** (Mar., 2007) 65015.
- [110] A. A. Fraisse, *Limits on defects formation and hybrid inflationary models with three-year WMAP observations*, *Journal of Cosmology and Astro-Particle Physics* **03** (Mar., 2007) 008.
- [111] N. Bevis and P. M. Saffin, *Cosmic string y-junctions: A comparison between field theoretic and Nambu-Goto dynamics*, *Physical Review D* **78** (July, 2008) 23503.
- [112] L. Pogosian, S. H. Tye, I. Wasserman, and M. Wyman, *Cosmic strings as the source of small-scale microwave background anisotropy*, *Journal of Cosmology and Astro-Particle Physics* **02** (Feb., 2009) 013.
- [113] R. Battye and A. Moss, *Updated constraints on the cosmic string tension*, *Physical Review D* **82** (July, 2010) 023521.
- [114] J. Dunkley et al., *The Atacama Cosmology Telescope: Cosmological Parameters from the 2008 Power Spectrum*, *Astrophysical Journal* **739** (Sept., 2011) 52.
- [115] Planck Collaboration, P. A. R. Ade, N. Aghanim, C. Armitage-Caplan, M. Arnaud, M. Ashdown, F. Atrio-Barandela, J. Aumont, C. Baccigalupi, A. J. Banday, and et al., *Planck 2013 results. XXV. Searches for cosmic strings and other topological defects*, *ArXiv e-prints 1303.5085* (Mar., 2013).
- [116] E. J. Copeland, L. Pogosian, and T. Vachaspati, *Seeking string theory in the cosmos*, *Classical and Quantum Gravity* **28** (Oct., 2011) 204009.
- [117] S. A. Sanidas, R. A. Battye, and B. W. Stappers, *Constraints on cosmic string tension imposed by the limit on the stochastic gravitational wave background from the European Pulsar Timing Array*, *Physical Review D* **85** (June, 2012) 122003.
- [118] A. Buonanno, *TASI Lectures on Gravitational Waves from the Early Universe*, *ArXiv e-prints gr-qc/0303085* (Mar., 2003).
- [119] S. Imez, V. Mandic, and X. Siemens, *Gravitational-wave stochastic background from kinks and cusps on cosmic strings*, *Physical Review D* **81** (May, 2010) 104028.

- [120] E. Witten, *Superconducting strings*, *Nuclear Physics B* **249** (1985) 557–592.
- [121] K. Miyamoto and K. Nakayama, *Cosmological and astrophysical constraints on superconducting cosmic strings*, *Journal of Cosmology and Astroparticle Physics* **7** (July, 2013) 12.
- [122] Y.-W. Yu, K.-S. Cheng, G. Shiu, and H. Tye, *Implications of fast radio bursts for superconducting cosmic strings*, *Journal of Cosmology and Astro-Particle Physics* **11** (Nov., 2014) 40.
- [123] J. J. Blanco-Pillado, K. D. Olum, and B. Shlaer, *Number of cosmic string loops*, *Physical Review D* **89** (Jan., 2014) 023512.
- [124] D. F. Chernoff and S. H. Tye, “to appear.”
- [125] V. Vanchurin, K. Olum, and A. Vilenkin, *Cosmic string scaling in flat space*, *Physical Review D* **72** (Sept., 2005) 63514.
- [126] M. Sakellariadou, *A note on the evolution of cosmic string/superstring networks*, *Journal of Cosmology and Astro-Particle Physics* **04** (Apr., 2005) 003.
- [127] C. J. Martins and E. P. Shellard, *Fractal properties and small-scale structure of cosmic string networks*, *Physical Review D* **73** (Feb., 2006) 43515.
- [128] A. Avgoustidis and E. P. Shellard, *Effect of reconnection probability on cosmic (super)string network density*, *Physical Review D* **73** (Feb., 2006) 41301.
- [129] C. Ringeval, M. Sakellariadou, and F. R. Bouchet, *Cosmological evolution of cosmic string loops*, *Journal of Cosmology and Astro-Particle Physics* **02** (Feb., 2007) 023.
- [130] J. Polchinski and J. V. Rocha, *Analytic study of small scale structure on cosmic strings*, *Physical Review D* **74** (Oct., 2006) 83504.
- [131] J. Polchinski and J. V. Rocha, *Cosmic string structure at the gravitational radiation scale*, *Physical Review D* **75** (June, 2007) 123503.
- [132] D. F. Chernoff and S. H. H. Tye, *Cosmic string detection via microlensing of stars*, *ArXiv e-prints 0709.1139* (Sept., 2007).
- [133] D. F. Chernoff, *Clustering of superstring loops*, *ArXiv e-prints 0908.4077* (Aug., 2009).
- [134] C. J. Hogan, *Runaway cosmic strings*, *Nature* **326** (Apr., 1987) 853–855.
- [135] C. J. Hogan and M. J. Rees, *Gravitational interactions of cosmic strings*, *Nature* **311** (Sept., 1984) 109–114.
- [136] T. W. B. Kibble, *Evolution of a system of cosmic strings.*, *Nuclear Physics B* **252** (1985) 227–244.

- [137] C. J. A. P. Martins and E. P. S. Shellard, *Scale-invariant string evolution with friction*, *Physical Review D* **53** (Jan., 1996) 575.
- [138] S. Kuroyanagi, K. Miyamoto, T. Sekiguchi, K. Takahashi, and J. Silk, *Forecast constraints on cosmic string parameters from gravitational wave direct detection experiments*, *Physical Review D* **86** (July, 2012) 023503.
- [139] S. Kuroyanagi, K. Miyamoto, T. Sekiguchi, K. Takahashi, and J. Silk, *Forecast constraints on cosmic strings from future CMB, pulsar timing, and gravitational wave direct detection experiments*, *Physical Review D* **87** (Jan., 2013) 023522.
- [140] J. Binney and S. Tremaine, *Galactic Dynamics: Second Edition*. Princeton University Press, 2008.
- [141] S. Liebes, *Gravitational lenses*, *Physical Review* **133** (Feb., 1964) 835–844.
- [142] B. Paczynski, *Gravitational microlensing by the galactic halo*, *Astrophysical Journal* **304** (May, 1986) 1–5.
- [143] S. Mao, *Astrophysical applications of gravitational microlensing*, *Research in Astronomy and Astrophysics* **12** (Aug., 2012) 947–972.
- [144] J. K. Bloomfield and D. F. Chernoff, *Cosmic string loop microlensing*, *Physical Review D* **89** (June, 2014) 124003.
- [145] M. S. Pshirkov and A. V. Tuntsov, *Local constraints on cosmic string loops from photometry and pulsar timing*, *Physical Review D* **81** (Apr., 2010) 083519.
- [146] “COROT: COncvection, ROtation & planetary Transits.” <http://smc.cnes.fr/COROT>, Sept., 2014.
- [147] “Rossi X-Ray Timing Explorer (RXTE): December 1995 - January 2012.” <http://heasarc.gsfc.nasa.gov/docs/xte/XTE.html>, Sept., 2014.
- [148] D. F. Chernoff, *White paper: Microlensing of superstring loops. unpublished document contributed to LSST*, 2009.
- [149] D. F. Chernoff, R. Graziani, A. Kwok, and T. Morris, “to appear.”
- [150] M. R. DePies and C. J. Hogan, “Harmonic gravitational wave spectra of cosmic string loops in the galaxy.” <http://adsabs.harvard.edu/abs/2009arXiv0904.1052D>, Apr., 2009.
- [151] K. Danzmann and T. A. Prince, “Mission documents [LISA International Science Team].” http://list.caltech.edu/mission_documents, 2011.
- [152] A. J. Farmer and E. S. Phinney, *The gravitational wave background from cosmological compact binaries*, *Monthly Notices of the Royal Astronomical Society* **346** (Dec., 2003) 1197–1214.